## DISCLAIMER

**This report was prepared as an account of work sponsored by an agency of the United States Government. Neither the United States Government nor any agency thereof, nor any of their employees, makes any warranty, express or implied, or assumes any legal liability or responsibility for the accuracy, completeness, or usefulness of any information, apparatus, product, or process disclosed, or represents that its use would not infringe privately owned rights. Reference herein to any specific commercial product, process, or service by trade name, trademark, manufacturer, or otherwise does not necessarily constitute or imply its endorsement, recommendation, or favoring by the United States Government or any agency thereof. The views and opinions of authors expressed herein do not necessarily state or reflect those of the United States Government or any agency thereof. Reference herein to any social initiative (including but not limited to Diversity, Equity, and Inclusion (DEI); Community Benefits Plans (CBP); Justice 40; etc.) is made by the Author independent of any current requirement by the United States Government and does not constitute or imply endorsement, recommendation, or support by the United States Government or any agency thereof.**

ANL-25/49

Argonne NATIONAL LABORATORY

# Computational Modeling of Water Infiltration From Ditches Into Roadway Embankments

Nuclear Science and Engineering Division

**About Argonne National Laboratory**
Argonne is a U.S. Department of Energy laboratory managed by UChicago Argonne, LLC under contract DE-AC02-06CH11357. The Laboratory's main facility is outside Chicago, at 9700 South Cass Avenue, Lemont, Illinois 60439. For information about Argonne and its pioneering science and technology programs, see www.anl.gov.

**DOCUMENT AVAILABILITY**

**Online Access:** U.S. Department of Energy (DOE) reports produced after 1991 and a growing number of pre-1991 documents are available free at OSTI.GOV (http://www.osti.gov/), a service of the US Dept. of Energy's Office of Scientific and Technical Information.

**Reports not in digital format may be purchased by the public from the National Technical Information Service (NTIS):**

U.S. Department of Commerce
National Technical Information Service
5301 Shawnee Road
Alexandria, VA 22312
**www.ntis.gov**
Phone: 800-553-NTIS (6847) or 703-605-6000
Fax: 703-605-6900
Email: **orders@ntis.gov**

**Reports not in digital format are available to DOE and DOE contractors from the Office of Scientific and Technical Information (OSTI):**

U.S. Department of Energy
Office of Scientific and Technical Information
P.O. Box 62
Oak Ridge, TN 37831-0062
**www.osti.gov**
Phone: 865-576-8401
Fax: 865-576-5728
Email: **reports@osti.gov**

**Disclaimer**
This report was prepared as an account of work sponsored by an agency of the United States Government. Neither the United States Government nor any agency thereof, nor UChicago Argonne, LLC, nor any of their employees or officers, makes any warranty, express or implied, or assumes any legal liability or responsibility for the accuracy, completeness, or usefulness of any information, apparatus, product, or process disclosed, or represents that its use would not infringe privately owned rights. Reference herein to any specific commercial product, process, or service by trade name, trademark, manufacturer, or otherwise, does not necessarily constitute or imply its endorsement, recommendation, or favoring by the United States Government or any agency thereof. The views and opinions of document authors expressed herein do not necessarily state or reflect those of the United States Government or any agency thereof, Argonne National Laboratory, or UChicago Argonne, LLC.

ANL-25/49

# Computational Modeling of Water Infiltration From Ditches Into Roadway Embankments

prepared by:

Marta Sitek and Steven Lottes
Nuclear Science and Engineering Division, Argonne National Laboratory

JULY 2026

# Table of Contents


1 Introduction ..... 1
2 Scope of the Study ..... 7
3 Computational Modeling ..... 9
3.1 Richards' Equation Based Software VS2DI ..... 9
3.2 Computational Fluid Dynamics Approach ..... 11
3.2.1 Validation Example: Watson's Experiment ..... 14
3.2.2 Verification Example: Jurin's Law ..... 19
4 Ditch-Embankment Infiltration Predictions ..... 23
4.1 Impact of Capillary Pressure ..... 25
4.2 Impact of Soil Porosity ..... 27
4.3 Impact of Grain Size ..... 28
4.4 Impact of Initial Moisture Content ..... 31
4.5 Impact of Groundwater ..... 32
4.6 Comparison of CFD and VS2D Results ..... 34
5 Conclusions ..... 37
6 Acknowledgements ..... 40
7 References ..... 41

# List of Figures

Figure 1-1 Maximum dry density, corresponding wet density and porosity of the typical SC soils. Refer to SC-T-29 for curve numbering. ..... 4

Figure 1-2 Saturated hydraulic conductivity vs. soil porosity for varying grain size. ..... 5

Figure 2-1 Typical half roadway cross section with marked freeboard clearance between the water surface in the ditch and the pavement subbase. ..... 7

Figure 3-1 A sketch of the extent of the soil (porous region, porosity < 1) and the space above it (fluid region, porosity = 1) in the proposed CFD model. ..... 11

Figure 3-2 A snapshot of the CFD model used in the computations. Symmetry surfaces are marked in blue; walls are marked in grey and pressure outlets are marked in orange. ..... 12

Figure 3-3 Comparison of the experimental findings by Watson and van Genuchten model. .... 15

Figure 3-4 Sketch of the soil sample and experimental set-up (left) and the discretization of the model and the lines used to record the solution (right). ..... 15

Figure 3-5 Hydraulic conductivity (a) and water content (b) along the height of the CFD model at 60 seconds of simulated time. ..... 16

Figure 3-6 CFD results from a model with flow-soil resistance independent of the water content compared with the experimental results by Watson. ..... 17

Figure 3-7 CFD results from a model with implemented van Genuchten model of water flow in unsaturated soils compared with the experimental results by Watson..... 18

Figure 3-8 Water content vs. hydraulic conductivity at 60 seconds of simulated time for the CFD model with variable conductivity and VS2D model compared to Watson's results..... 18

Figure 3-9 Capillary rise of water in a tube. The water level at the end of the simulation, a close-up view of the meniscus, and a plot of the rise of water level in time compared to the Jurin's law. ..... 19

Figure 3-10 Model used to analyze the capillary rise in porous media. ..... 20

Figure 3-11 Volume fraction of water in a tube filled with porous medium at steady state, left-contour plot on a plane section through the computational domain, right- point plot along the tube centerline. ..... 21

Figure 3-12 Capillary rise dependence on grain size and soil porosity. ..... 21

Figure 4-1 Geometry of the base case model. ..... 23

Figure 4-2 Discretization of an example CFD model with a refinement at the border between regions of different porosity. ..... 23

Figure 4-3 Volume fraction of water in the base case at 1 minute of simulated time. ..... 24

Figure 4-4 Volume fraction of water in the base case at 10 minutes of simulated time. ..... 24

Figure 4-5 Volume fraction of water in the base case at 20 minutes of simulated time. ..... 24

Figure 4-6 Comparison of the extent of infiltration within a minute of simulated time in the model (a) without and (b) with capillary pressure. ..... 25

Figure 4-7 Comparison of the extent of infiltration within 10 minutes of simulated time in the model (a) without and (b) with capillary pressure. ..... 26

Figure 4-8 Progress of the infiltration in the model with capillary pressure after 20 minutes of simulated time. ..... 26

Figure 4-9 Impact of soil porosity on the infiltration extent. ..... 27

Figure 4-10 Water infiltration at 1hr of simulated time. Soil compaction is 95%, grain size varies. ..... 28

Figure 4-11 Close-up view of the infiltration near the top edge of the ditch. ..... 29

Figure 4-12 Infiltration at various times for soil grain size 1 mm and porosity 5%. ..... 30

Figure 4-13 Impact of initial soil moisture content on water inflitration. ..... 31

Figure 4-14 Saturation at various times in a case with water table at the ditch bottom, soil porosity 5%, and grain size 0.25 mm and 2 mm. ..... 32

Figure 4-15 Saturation at 10 hours of simulated time in the case with water table at the ditch bottom, soil porosity 5%, and grain size 2 mm..... 33

Figure 4-16 Saturation at various times in a case with water table at the ditch bottom, soil porosity 40%, and grain size 0.25 mm..... 33

Figure 4-17 Comparison of results from CFD and VS2D at 1hr of simulated time. Grain size 1 mm, soil porosity 5%. Note: the color bars differ between the software; blue color means full saturation in both codes; VS2D plot covers only the soil, and CFD covers both soil and the volume above it. ..... 34

Figure 4-18 Comparison of results from CFD vs. VS2D at 1hr of simulated time. Grain size is 0.1 mm, porosity 5%. ..... 34

Figure 4-19 Comparison of results from CFD vs. VS2D at 1hr of simulated time. Grain size is 2 mm, porosity 20%. ..... 35

Figure 4-20 Comparison of the infiltration at 1 hr (left) and 24 hr (right) of the simulation in VS2D. Grain size is 1 mm, soil porosity 5%..... 35

Figure 4-21 Comparison of the infiltration at 1 hr (left) and 24 hr (right) of the simulation in VS2D. Grain size is 0.01 mm, porosity 5%. ..... 36

# List of Tables

Table 1-1. USDA particle size classes. ..... 2
Table 1-2. Typical porosity ranges by USDA texture class. ..... 3
Table 1-3 Saturated hydraulic conductivity classification according to NRCS. ..... 4
Table 1-4 Capillary rise for various soil textures ..... 6
Table 2-1 Parameter values considered in the study. ..... 7
Table 3-1 The van Genuchten equation parameters for generic soil classes ..... 10
Table 3-2 Capillary rise in porous media. ..... 22
Table 5-1 Summary of results ..... 38

**Nomenclature**

| Symbol | Description | Units |
|---|---|---|
| $\bar{A}$ | Specific area | $m^2$ ($ft^2$) |
| $C$ | Coefficient in eq. (1.2) | $m^{-1}s^{-1}$ ($ft^{-1}s^{-1}$) |
| $C_H$ | Coefficient in eq. (1.3) | - |
| $d_{10}$ | Grain size that represents 10% of grains smaller than $d_{10}$ | m (ft) |
| $d_p$ | Equivalent particle diameter | m (ft) |
| $h$ | Height | m (ft) |
| $k$ | Hydraulic permeability | $m^2$ ($ft^2$) |
| $k_s$ | Saturated hydraulic permeability | $m^2$ ($ft^2$) |
| $K$ | Hydraulic conductivity | m/s (ft/s) |
| $K_r$ | Relative hydraulic conductivity | m/s (ft/s) |
| $K_s$ | Saturated hydraulic conductivity | m/s (ft/s) |
| $L$ | Length | m (ft) |
| $m$ | Coefficient in eq. (3.9) | - |
| $p$ | Pressure | Pa ($lb/ft^2$) |
| $r$ | Radius | m (ft) |
| RMC | Residual moisture content | - |
| $s_e$ | Effective saturation | - |
| $v$ | Bulk velocity | m/s (ft/s) |
| $v_s$ | Superficial water velocity | m/s (ft/s) |
| VMC | Volumetric moisture content | - |
| $\alpha$ | Coefficient in eqs. (3.2), (3.3) | - |
| $\beta$ | Coefficient in eqs. (3.2), (3.3) | - |
| $\theta$ | Contact angle | - |
| $\phi$ | Relative volume fraction of water | - |
| $\phi_w$ | Volume fraction of water | - |
| $\phi_{w,r}$ | Residual fraction of water | - |
| $\phi_{w,s}$ | Saturated fraction of water | - |
| $\mu$ | Dynamic viscosity of water | Pa-s (lbf-s/$ft^{2)}$ |
| $\rho$ | Water density | $kg/m^3$ ($lb/ft^3$) |
| $\chi$ | Porosity | - |
| $\sigma$ | Surface tension of water | Pa (lb/ft2) |

# 1 Introduction

Ditches are built along roadways to convey the stormwater runoff. They collect the runoff from the pavement and adjacent drainage areas. Water can move freely in a ditch away from the road surface, thus making it safer for the vehicular traffic.

South Carolina DOT expressed interest in studying infiltration of water from ditches into roadway embankments. As part of the current design criteria [1], it is recommended that the road subgrades be 1.0 foot above the design event water surface elevation in the ditch. The distance between the water surface and bottom of the subbase is referred to as “freeboard”. The purpose of this requirement is to lower the risk of pavement damage by moving the flow away from the pavement, containing the captured flow, and conveying flow received from adjacent properties to outfalls. With changes in roadway design standards, larger shoulders and flatter cross-slopes have moved ditches further away from the pavement and the subbase. These changes could allow for a lower freeboard standard without reducing safety margins due to the increased lateral distance from the subbase to the ditch.

The objective of this study is to evaluate whether the current SCDOT criterion requiring the roadway subgrade to be 1 ft above the design-event ditch water surface can be relaxed under selected geometric and soil conditions, particularly where larger shoulder widths and flatter side slopes increase horizontal separation between ditch water and pavement structure.

Computational fluid dynamics (CFD) was selected in this study not because it is the simplest approach for unsaturated flow in soils, but because it provides a unified framework for representing both the open-water region in the ditch and the adjacent porous embankment. In particular, the CFD formulation allows the ditch water, the air above it, and the water-air mixture within the soil pores to be modeled within a single domain, while also capturing the free surface in the ditch explicitly. This approach is attractive for problems in which the interaction between surface water and subsurface flow is of interest, and it offers flexibility for future application to more complex geometries or additional coupled processes.

At the same time, the present CFD model should be viewed as an engineering approximation of flow in porous media. The soil is represented as a continuum porous region with effective properties such as porosity and flow resistance rather than as an explicit pore-scale geometry. As a result, the method does not replace Richards-equation-based formulations, which remain the more natural and computationally efficient approach for unsaturated flow in soils alone. For this reason, VS2DI was also used in the study as a reference porous-media model and as a basis for comparison.

Several assumptions were adopted to make the problem tractable and to support a screening-level assessment of seepage behavior. First, the water level in the ditch was held constant throughout each simulation. This assumption is conservative because it maintains the maximum hydraulic head along the ditch boundary for the full event duration and therefore tends to overpredict infiltration relative to a transient storm hydrograph in which ditch water depth would rise and fall with time. The resulting seepage extent should therefore be interpreted as an upper-bound estimate for the specified conditions.

Second, the analysis adopts a quasi-two-dimensional representation of the problem by assuming that geometry and flow conditions are sufficiently uniform along the ditch that infiltration can be approximated from a representative cross section. This assumption is most appropriate where ditch geometry, water depth, and surrounding soil conditions vary slowly in the longitudinal direction.

Third, the porous-medium representation idealizes the embankment soil using effective properties derived from porosity, hydraulic resistance, and a characteristic grain size. In the CFD formulation, this corresponds to an equivalent medium that is closer to a packed bed of uniform particles than to a natural or compacted field soil. Real embankment soils contain a distribution of particle sizes rather than a single uniform grain size, and their hydraulic behavior depends on gradation, soil fabric, structure, and compaction history. Accordingly, the present results should be interpreted primarily as a trend and bounding study rather than as a site-specific prediction for a particular embankment.

Finally, the present model addresses hydraulic moisture migration only. It does not include deformation of the soil skeleton or coupling to geo-mechanical response. Therefore, the simulations do not directly predict changes in strength, pavement support, internal erosion potential, slope stability, or damage associated with repeated wetting and drying cycles. Those issues require separate geotechnical evaluation.

Movement of water into soil (infiltration) and water movement in soil (percolation and capillary action) are caused by two driving forces: gravity force and capillary forces. The flow caused by these forces is characterized by permeability, porosity, hydraulic conductivity for the gravity force and by adhesion, cohesion, and surface tension forces for capillary action forces [2].

The soil infiltration rate is the rate at which water enters the soil and is related to the rate water can move through soil and its layers. It depends on texture, structure, initial moisture levels, among others. Soil infiltration rate depends strongly on soil texture because texture controls pore size distribution and connectivity. Large, well-connected macropores between sand grains (coarse texture) let water enter quickly. Loamy soil exhibits moderate infiltration because the balance of macro- and micropores supports decent intake without extremely fast drainage. Silty soils have moderate to low infiltration due to medium-to-small pores, and they can be prone to surface sealing/crusting under rainfall, which sharply reduces infiltration. Clayey soils (fine texture) often exhibit low infiltration because they are dominated by tiny micropores which have high water-holding capacity but slow water entry. Soil structure, which defines how particles are aggregated into clusters and how pores are arranged, can change infiltration as much as—or more than—texture, because infiltration is controlled mainly by the size, continuity, and stability of pores near the surface. Well-aggregated granular soils have many connected large pores between aggregates, letting water enter quickly. Poor/weak structure reduces infiltration. Structureless, single-grain but compacted, or weakly aggregated soils have fewer connected macropores, so water enters more slowly. Initial soil moisture strongly affects infiltration because it changes the soil suction and how quickly the soil becomes saturated near the surface. Drier soil has higher initial infiltration rate which declines during a storm event. Wetter soil has lower initial infiltration rate. The soil reaches near-saturation sooner, so infiltration becomes limited mainly by the soil's hydraulic conductivity. Soil particles vary greatly in size. A USDA classification for mineral fraction <2 mm [3] is presented in Table 1-1.

**Table 1-1. USDA particle size classes.**

| Separate | Diameter (mm) |
|---|---|
| Very coarse sand | 2.0 – 1.0 |
| Coarse sand | 1.0 – 0.5 |
| Medium sand | 0.5 – 0.25 |
| Fine sand | 0.25 – 0.10 |
| Very fine sand | 0.10 – 0.05 |
| Silt | 0.05 – 0.002 |
| Clay | < 0.002 |

Soil permeability is affected by porosity, which is the volume fraction of pore space, as well as the type and size of pores. Properties that affect porosity are organic matter levels, aggregation (arrangement of primary soil particles: sand, silt, and clay, around soil organic matter and through particle associations), and shrinking and swelling of clay particles (some clayey soils develop cracks as they dry). Porosity variation depending on the soil type is presented in Table 1-2 .

**Table 1-2. Typical porosity ranges by USDA texture class.**

| Soil texture (USDA) | Typical total porosity (%) |
|---|---|
| Sand | 35–45 |
| Loamy sand | 35–45 |
| Sandy loam | 40–50 |
| Loam | 45–55 |
| Silt loam | 45–55 |
| Silt | 45–55 |
| Sandy clay loam | 40–50 |
| Clay loam | 40–55 |
| Silty clay loam | 45–55 |
| Sandy clay | 40–50 |
| Silty clay | 45–55 |
| Clay | 45–60 |

Soil compaction is a process in which stress is applied to soil and presses the particles together, reducing pore space between them. Heavily compacted soils contain few large pores, less total pore volume and, consequently, have greater bulk density. Soil compaction increases soil strength, which is the ability of soil to resist being moved by an applied force and reduces the rate of water infiltration and drainage. The depositional porosity of well-sorted clean sand is in the range 0.50–0.70. Compaction reduces it to a residual porosity of 0.25–0.40. Mechanical compaction is very efficient in shales and mudstones for which the porosity decreases from the depositional porosity 0.60–0.70 to a residual porosity 0.05–0.10 [4].

Section 205.3.2 of the SCDOT Construction Manual [6] specifies the requirements for embankment soil compaction. During the formation and compaction of an embankment, each lift must be compacted to a minimum 95% of maximum dry density. Maximum dry density and optimum moisture content should be determined using the One-Point Proctor Method [7] or the field method of determining the moisture-density relationship [8].

Maximum dry density is the dry density obtained by the compaction of soil at its optimum moisture content. Figure SC-T-29A (SC-T-29) presents wet density vs. moisture content curves for typical soils in South Carolina, as well as a table with maximum dry density and optimum moisture content for a set of 27 soil types, see Table 6. These two properties were used to calculate the wet density of the soil with the optimum moisture content, and its porosity. The results are presented in Figure 1-1.

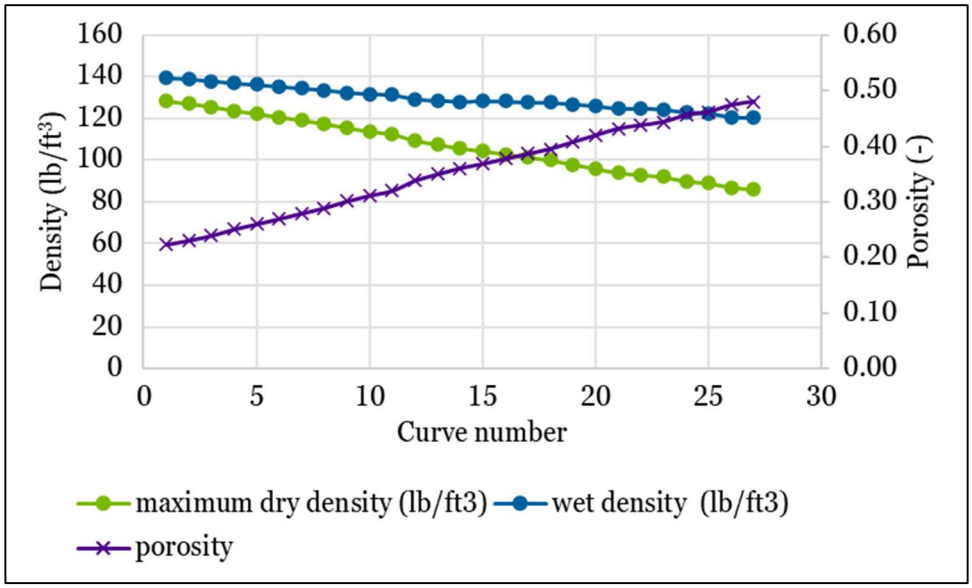



**Figure 1-1 Maximum dry density, corresponding wet density and porosity of the typical SC soils. Refer to SC-T-29 for curve numbering.**

Hydraulic conductivity, $K$(m/s), is related to permeability as follows

$$K = \frac{k\rho g}{\mu}, \tag{1.1}$$

where $k$ is hydraulic permeability (unit m$^2$), $\rho$ is water density (998.2 kg/m$^3$ at 20 °C and atmospheric pressure), $g$ is the gravitational acceleration (9.81 m/s$^2$), and $\mu$ is water dynamic viscosity ($1.0016 \cdot 10^{-3}$ Pa·s at 20 °C and atmospheric pressure) [9].

Table 1-3 shows a saturated hydraulic conductivity classification adopted by USDA NRCS [10].

**Table 1-3 Saturated hydraulic conductivity classification according to NRCS.**

| $K_{sat}$ Class | Criteria | |
|---|---|---|
| | [cm/hr] | [in/hr] |
| Very low | <0.0036 | <0.001417 |
| Low | 0.0036-0.036 | 0.001417-0.01417 |
| Mod. Low | 0.036-0.36 | 0.01417-0.1417 |
| Mod. High | 0.36-3.6 | 0.1417-1.417 |
| High | 3.6-36 | 1.417-14.17 |
| Very high | >36.0 | >14.17 |

Hydraulic conductivity depends on the size of the smallest fraction, the gradation of the grains, and their shape. Most formulations found in the literature estimate the saturated hydraulic conductivity of soil as a function of the $d_{10}$ squared:

$$K = Cd_{10}^2 \tag{1.2}$$

where $C$ is a coefficient with dimensions m$^{-1}$s$^{-1}$, and $d_{10}$ is grain size that represents the 10% of grains smaller than $d_{10}$.

The earliest empirical equation for the estimation of saturated hydraulic conductivity as a function of particle size is attributed to Hazen [11]:

$$K = C_H \frac{\rho g}{\mu} d_{10}^2 \tag{1.3}$$

where $C_H$ is a dimensionless coefficient, usually equals 1.0, and $d_{10}$ (m) is grain size that represents the 10% of grains smaller than $d_{10}$.

Another widely used formula is attributed to Kozeny and Carman [12][13]:

$$K = \frac{1}{180} \frac{\rho g}{\mu} \frac{\chi^3}{(1-\chi)^2} d_{10}^2 \tag{1.4}$$

where $\chi$ is porosity (void ratio). Hydraulic conductivity is higher in saturated than in unsaturated soil. It is common to assume that conductivity is the same in the horizontal and vertical directions.

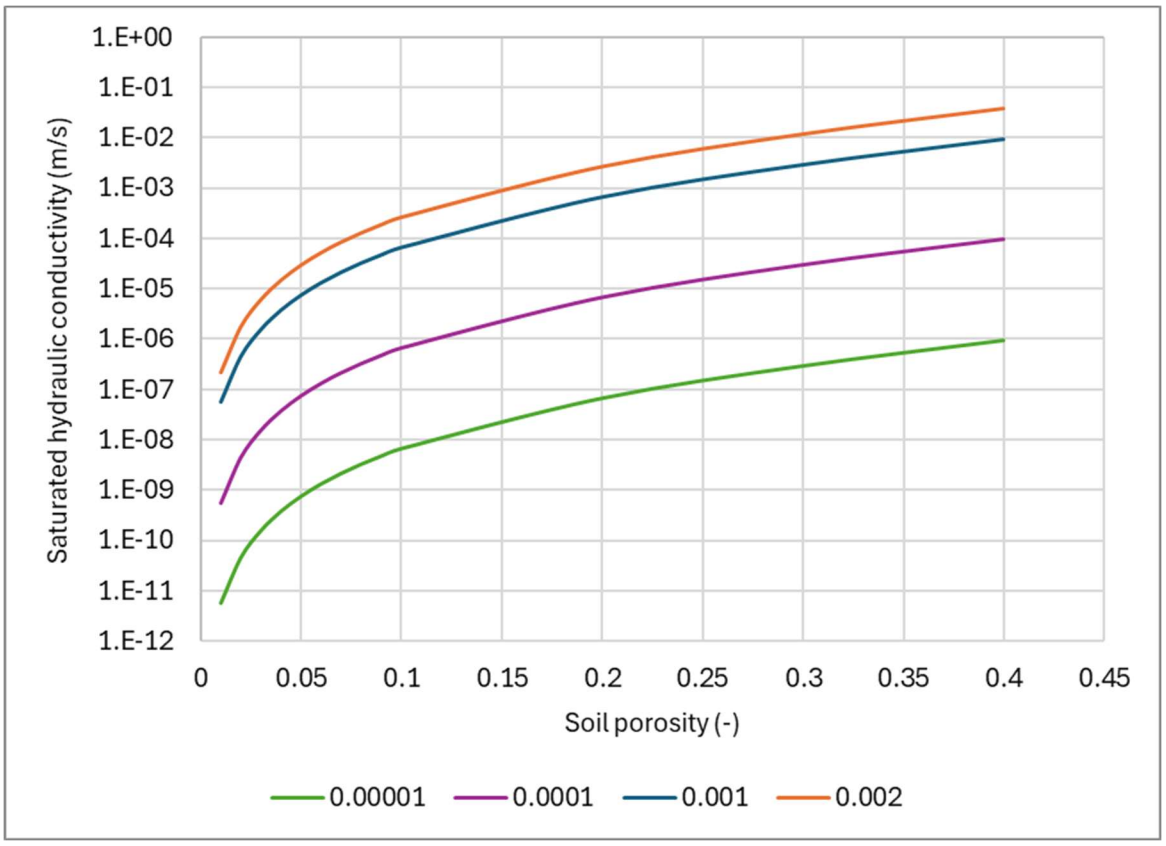



**Figure 1-2 Saturated hydraulic conductivity vs. soil porosity for varying grain size.**

Capillary rise is the upward movement of water between soil particles due to a combination of its cohesion and adhesive forces between the water and particle surfaces. In fine soil, the upward movement of water is slow, but covers a long distance. On the other hand, in coarse soil, the upward movement of water is quick, but covers only a short distance. Capillary rise for different soil textures is presented in Table 1-4 [14].

**Table 1-4 Capillary rise for various soil textures**

| Soil texture | Capillary rise |
|---|---|
| coarse (sand) | 20 to 50 cm (8 - 20 in) |
| medium | 50 to 80 cm (20 – 31.5 in) |
| fine (clay) | 80 cm up to several meters (31.5 in) |

Capillary rise is controlled not only by soil texture but also by pore-size distribution, soil structure, and boundary conditions in the sample or field setting [15].

# 2 Scope of the Study

A sketch of a half of a typical roadway cross section is shown in Figure 2-1 with the primary elements and relative locations. In the current study it is assumed that the subbase is only under the travel lanes; in the case of travel lanes with a paved shoulder, the extent of the subbase increases.

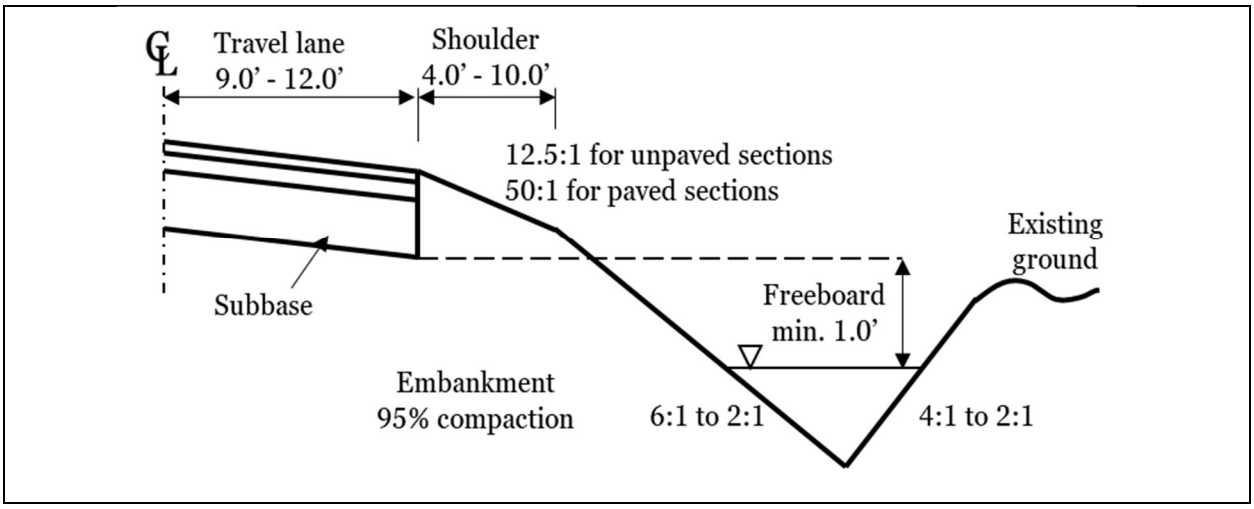



**Figure 2-1 Typical half roadway cross section with marked freeboard clearance between the water surface in the ditch and the pavement subbase.**

This study covers several parameters, presented in Table 2-1 along with a range of values to be tested.

**Table 2-1 Parameter values considered in the study.**

| | Parameter | Value range |
|---|---|---|
| Water conditions | Initial moisture content (%) | 0 - 30 |
| | Freeboard (ft) | -1, 0, 1 |
| | Water table (ft) (distance from the bottom of the ditch) | 0, 1, none |
| Soil properties | Porosity (%) | 5 - 40 |
| | Particle size | 0.001 – 2 mm |
| Geometry | Shoulder width | 4, 10 ft |
| | Shoulder slope | 12.5:1 |
| | Ditch front slope | 4:1 |
| | Ditch back slope | 4:1 |
| Time | Time of flow duration in ditch | up to 24 hours |

In the base case, the embankment is built of sandy soil with zero initial moisture, a porosity of 0.4 and grain diameter of 0.2 mm. The horizontal distance between the edge of the subbase and water free surface edge is 10 ft (4 ft shoulder at 12.5:1 slope plus 6 ft 8 in ditch 4:1 slope).

Next, the parameters are varied separately from those of the base case. The geometry of the model is rebuilt for freeboard values different from the base case. The analysis covers a simulated time

period of 24 hours or less. If the infiltration rate is high enough for the waterfront to reach the subbase within a shorter time, the analysis is terminated.

The analysis assumes that the water is at maximum height in the ditch for the entire time period. This approach yields worst case, conservative results because the static pressure driving water into the soil at the sides and bottom of the ditch is also at a maximum. Varying water heights over time could be modeled, but then the time history of the water height would have to be provided. To maintain water height, the water seeping into the surrounding soil is replaced in the ditch by adding a volume source to the differential equations. This source term replaces the inflow from the upstream of the water in the ditch needed to keep the water level constant since that inflow is not modeled to save computer resources and time.

# 3 Computational Modeling

Several levels of assessment were used to build confidence in the CFD approach adopted in this study. First, a code/model verification check was performed for capillary rise in a narrow tube by comparing the computed rise with the analytical result given by Jurin's law. This comparison tests whether the numerical treatment of interfacial forces and pressure balance reproduces the expected capillary behavior in a simple geometry.

Second, an assessment was performed for unsaturated porous-medium behavior by comparing the predicted hydraulic conductivity–water content relationship with the experimental data reported by Watson [22] for drainage of a sand column. This comparison evaluates whether the adopted porous-medium resistance formulation, including the water-content-dependent conductivity relationship, reproduces the observed behavior of unsaturated flow.

Third, the ditch-embankment infiltration predictions from CFD were compared with those from VS2DI, a Richards-equation-based porous-flow model commonly used for variable-saturation problems. This comparison is not a formal validation against field measurements, but rather a cross-model consistency check. For the representative cases examined, the two approaches produced similar infiltration patterns and comparable wetting-front extents, with differences that were small relative to the scale of the ditch-embankment geometry.

## 3.1 Richards' Equation Based Software VS2DI

VS2DI is a software package for simulating water, solute, and heat transport through soils or other porous media under conditions of variable saturation. The package contains a graphical preprocessor for constructing simulations, a postprocessor for displaying simulation results, and numerical models that solve for flow and solute transport (VS2DT) and flow and heat transport (VS2DH). Flow is described by the Richards equation, and solute and heat transport are described by advection-dispersion equations; the finite-difference method is used to solve these equations. Problems can be simulated in one, two, or three (assuming radial symmetry) dimensions [17].

Voids in unsaturated soil are occupied by water and air. In the case of fully saturated soils, the flow of water follows Darcy's law. However, in the case of unsaturated soil, the flow of water and air must be considered simultaneously. Water in unsaturated soil does not flow through the air in the voids but flows along a flow path consisting of continuous water. Accordingly, water flow is dependent on the degree of saturation of the soil, and the hydraulic conductivity of an unsaturated soil is closely related to the water retention curve properties.

Five options are available in VS2DI [17] for describing the soil-water retention and relative hydraulic conductivity curves in unsaturated soils, including the Van Genuchten equation, among others. The Van Genuchten equation was selected for the current study, because the parameters were available for generic soil texture classes.

The effective saturation, $s_e$, represents the fraction of the pore space that is filled with water, relative to the total pore space available for water movement, and is defined as:

$$s_e = \frac{VMC - RMC}{porosity - RMC} \tag{3.1}$$

where $VMC$ is volumetric moisture content, $RMC$ is residual moisture content, and which for a zero residual water content, simplifies to the ratio of volumetric moisture content and porosity.

The residual moisture content, *RMC*, represents the fraction of soil void space occupied by water that is held so strongly by the soil that it is essentially immobile under the action of typical hydrological forces like gravity, pressure, and capillary forces. and adsorptive forces binding a thin film of water to the surface of soil particles with strong intermolecular forces. The effective saturation, $s_e$, is therefore the fraction of space filled by water that can be moved, i.e., flow.

The relative hydraulic conductivity, $K_r$, is the ratio of the unsaturated hydraulic conductivity to saturated conductivity. For a negative pressure head, $h < 0$, the effective saturation and relative hydraulic conductivity are equal to [17]:

$$s_e = \frac{1}{(1 + |\alpha h|^{\beta})^{\gamma}} \tag{3.2}$$

$$K_r = \frac{\left(1 - |\alpha h|^{\beta-1}\left(1 + |\alpha h|^{\beta}\right)^{-\gamma}\right)^2}{(1 + |\alpha h|^{\beta})^{0.5\gamma}} \tag{3.3}$$

where $\alpha$, $\beta$, and $\gamma = 1 - 1/\beta$ are parameters which need to be estimated experimentally for each soil type. Negative pressure head refers to tension forces in the water in contact with unsaturated soil per unit area that would cause water at atmospheric pressure to be sucked up into the soil and held against the force of gravity. These parameters are available in VS2DI for generic soil texture classes. For saturated soil, the effective saturation and relative hydraulic conductivity are both equal to one: $s_e = 1, K_r = 1$.

**Table 3-1 The van Genuchten equation parameters for generic soil classes**

| | Medium sand | Fine sand | Sandy loam | Silt loam | Yolo light |
|---|---|---|---|---|---|
| Saturated hydraulic conductivity, $K_{hh}$ (m/s) | 0.00463 | 2.43e-5 | 8.1e-6 | 2.6e-6 | 1.3e-7 |
| Ratio of vertical to horizontal hydraulic conductivity, $K_{zz}/K_{hh}$ | 1 | 1 | 1 | 1 | 1 |
| Specific storage | 1e-4 | 1e-4 | 1e-4 | 1e-4 | 1e-4 |
| Porosity | 0.375 | 0.377 | 0.496 | 0.43 | 0.495 |
| Residual moisture content, RMC | 0.02 | 0.072 | 0.15 | 0.17 | 0.175 |
| $\alpha$ | 4.31 | 1.04 | 0.847 | 0.505 | 2.49 |
| $\beta$ | 3.1 | 6.9 | 4.8 | 7.0 | 1.6 |

## 3.2 Computational Fluid Dynamics Approach

Computational fluid dynamics (CFD) analysis solves the partial differential equations governing fluid motion (water and air in this application). The governing equations are the conservation of mass and Newton's 2nd law, expressing that acceleration (or deceleration) of the fluid times the fluid mass is equal to the applied force. Applied forces for a fluid can be pressure, shear, and gravity. A CFD model is a 3-dimensional section of the world, called the domain, with known conditions at its boundaries: zero velocity at solid surfaces, specified velocity at inlet boundaries, and pressure or zero gradients at outlet boundaries. The case of interest here, water infiltration from a ditch into the soil, can be simplified by assuming that the component of velocity of water in the ditch in the direction of the flow is zero. This can be done because the infiltration rate can reasonably be assumed to be independent of the velocity along the ditch. The water height in the ditch is also assumed to be constant. In this case a long section of ditch does not need to be modeled and can be reduced to a thin section, see Figure 3-1.

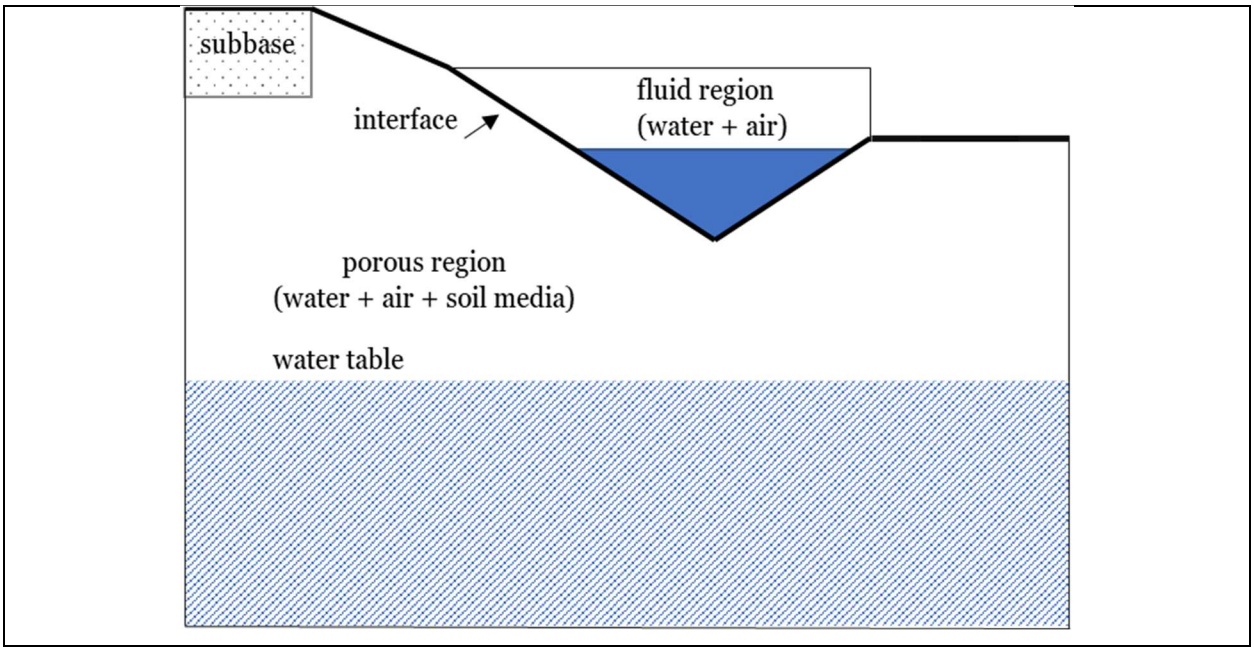



**Figure 3-1 A sketch of the extent of the soil (porous region, porosity < 1) and the space above it (fluid region, porosity = 1) in the proposed CFD model.**

Figure 3-2 shows an example of a CFD model for the region of interest. It is a thin slice through the volume of interest, meaning the roadway, ditch, and the space above and below them. The cross-sectional planes, normal to the page in the figure, are symmetry boundaries (marked in blue). The symmetry boundary condition defines a plane of reflection which assures that the flow field pattern is mirrored across that surface with no flow across those surfaces and no shear stress parallel to the surfaces. Using a domain with symmetry boundaries normal to the direction of ditch flow allows a computational domain much smaller than one needed to include flow in the longitudinal direction of the ditch, thus greatly reducing the time and computer resources needed to solve the problem. The top surface is a pressure outlet at atmospheric pressure. The side and bottom surfaces are pressure outlet boundary conditions with back-pressure set equal to the static pressure created by the fluid column above any position on those boundaries. Therefore, water can leave the ditch under the force of gravity, infiltrate the soil at the bottom of the ditch and push air in the soil along in front of it. Pressure does not build up in the soil due to water displacing air because the pressure boundary conditions on the sides of the domain allow the air to escape

through those boundaries. The interface between the fluid and porous region is an internal interface that allows for movement of fluid between the regions with different properties.

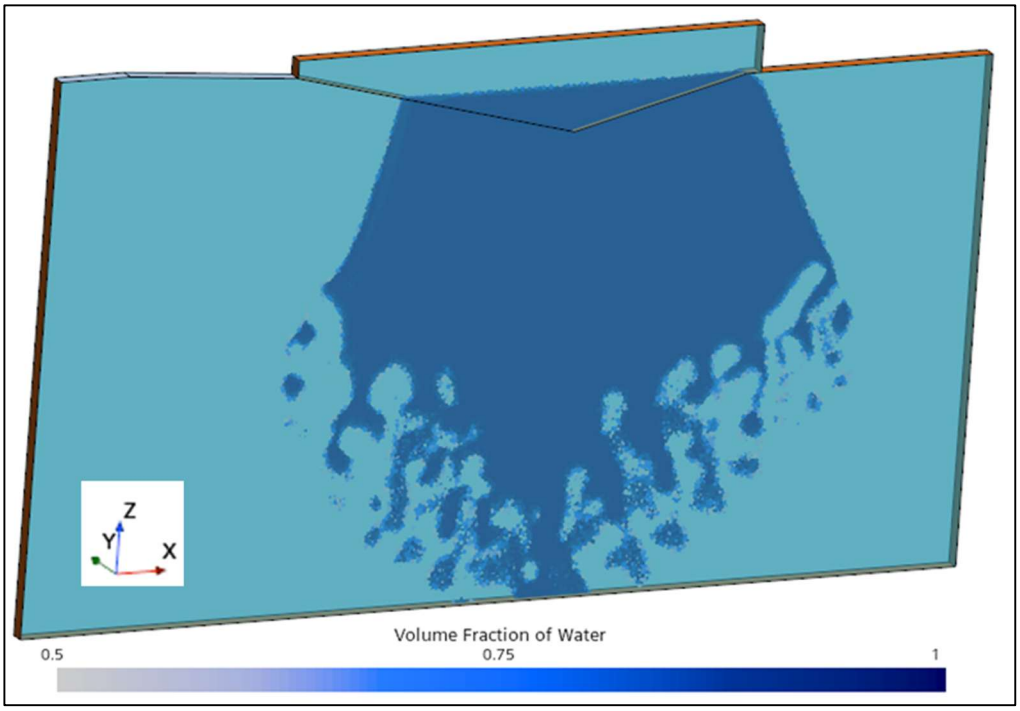



**Figure 3-2 A snapshot of the CFD model used in the computations. Symmetry surfaces are marked in blue; walls are marked in grey and pressure outlets are marked in orange.**

The solution is transient, i.e., changing during the simulation because it tracks the penetration and movement of water from the ditch into the soil over time. Depending on the infiltration rate, the flow may be laminar or turbulent. The Unsteady Reynolds-Averaged Navier-Stokes Solver was selected with Two-Layer Realizable K-Epsilon turbulence model to solve the flow. The time step differs depending on the flow velocity and varies from a fraction of a second to a few seconds. The simulation is run until one of two conditions is met: (1) the maximum horizontal extent of the water infiltrating the soil from the ditch moves past the bottom of the subbase, or (2) the maximum assumed time of a rain event of 24 hours is achieved.

The Eulerian two-phase model with a gas phase, air, and liquid phase, water, combined with the Volume of Fluid (VOF) physics model was selected to model the water flow with a free surface. The moisture content in the soil volume is defined using an initial condition of a specified volume fraction of water and air. Gravitational force is included in the model.

The water table within the embankment is also accounted for in the modeling. This level is considered one of the parameters because it influences the flow through the embankment. The volume fraction of air within the zone of the water table is equal to zero.

The soil volume can be modeled in various ways. An approach previously used by the authors to model permeable pavements is to use the Eulerian Multiphase model with two phases: water and air, and Volume of Fluid approach to compute the interface between the two phases. In CFD, soil is often idealized as a porous medium so that flow and transport can be modeled using volume-averaged continuum equations with permeability and porosity as effective properties [18]. This approach was adopted for this study.

A porous medium is characterized by three main parameters: porosity, porous inertial resistance, and porous viscous resistance. The resistance to flow within the porous media is related to the surface area per unit volume, which is determined from the aggregate size and porosity. The porous resistance was estimated from the Ergun relationship between pressure drop over a length, $L$, of a porous region and fluid velocity for a packed bed of spheres [19]:

$$-\frac{\mathrm{d}p}{L} = P_v v_s + P_i v_s^2 \tag{3.4}$$

$$P_v = \frac{150\mu(1-\chi)^2}{\chi^3 d_p^2}, \qquad P_i = \frac{1.75\rho(1-\chi)}{\chi^3 d_p} \tag{3.5}$$

where $P_v$ is the viscous term, $P_i$ is the inertial term, $\rho$ is fluid density, $\mu$ is fluid dynamic viscosity, $\chi$ is the porosity, $v_s$ is fluid superficial velocity through the medium ($v_s = \chi v$), $v$ is the mean physical velocity in the direction of flow, and $d_p$ is the equivalent particle diameter (aggregate size). When the saturated permeability $k_s$ or saturated conductivity $K_s$ of the medium is known, noting that $k_s = \mu K_s/(\rho g)$, the pressure drop can be calculated from Darcy's law:

$$-\frac{\mathrm{d}p}{L} = \frac{\mu}{k} v_s = \frac{\rho g}{K_s} v_s \tag{3.6}$$

Combining equations (3.4) and (3.6) gives the formulas for the equivalent particle diameter:

$$d_p = \sqrt{\frac{150(1-\chi)^2 k_s}{\chi^3}} \tag{3.7}$$

and

$$d_p = \sqrt{\frac{150\mu(1-\chi)^2 K_s}{\chi^3 \rho g}} \tag{3.8}$$

The definition of the porous medium resistance assumes constant permeability, and therefore conductivity, equal to the saturated state. In unsaturated flows the flow resistance increases due to the presence of air. Researchers proposed various empirical models of hydraulic conductivity as a function of the reduced saturation. One of the widely used relationships is that of Genuchten [17]:

$$K(\theta) = K_s \sqrt{\phi} \left[1 - \left(1 - \phi^{\frac{1}{m}}\right)^m\right]^2 \tag{3.9}$$

where the relative volume fraction of water is

$$\phi = \frac{\phi_w - \phi_{w,r}}{\phi_{w,s} - \phi_{w,r}} \tag{3.10}$$

with $\phi_w$ is the volume fraction of water, and $\phi_{w,s} = 1$ and $\phi_{w,r}$ are the saturated and residual volumetric water content, respectively, and m is a constant derived empirically for each soil type.

The viscous porous resistance is redefined as:

$$P_v(\phi) = \frac{K_s}{K(\phi)} P_v \tag{3.11}$$

### 3.2.1 Validation Example: Watson's Experiment

As a part of the validation of the CFD models used in this study, the above modifications of the soil resistance were incorporated into the porous media model and their impact on the CFD results was evaluated using an example case found in literature.

Watson [22] published results of an experimental study of the hydraulic conductivity in unsaturated soils. The researchers determined the conductivity vs. water content relationship from measurements obtained during drainage of an initially saturated sand column. A well-rounded sand fraction of 150-300 microns was used. The sand column was 57-cm-tall, with a cross-section 10 cm by 15 cm. The saturated water content was 0.35 and the room temperature was 69 F. Initially in the experiment, a steady-state saturated condition was achieved, then water was drained from the sand column to the atmosphere. In Watson's experiment, water content profiles were determined gravimetrically by measuring the amount of water remaining in different sections of the sand column at selected times during drainage. These moisture measurements, together with suction data, were used in the instantaneous profile method to estimate unsaturated hydraulic conductivity.

Firstly, the van Genuchten model was calibrated to approximate Watson's findings. The two sets of data points, showing the relationship between the water content and the hydraulic conductivity, are presented in Figure 3-3.

Next, a model representing the geometry and flow conditions from the experiment was constructed. A block of the size of the experimental sample was meshed out with polyhedral surface mesh with element target size of 2.5 mm and minimum size of 1 mm. The surface mesh was extruded through 1000 layers which resulted in ~2.5 million volume cells. Water content and hydraulic conductivity were calculated and saved along a grid of 7 by 7 vertical lines away from the walls of the model every 10 seconds of simulated time. The simulation was run until 20 minutes of the simulated time had passed. Figure 3-4 shows a sketch of the soil sample tested by Watson that is represented in the CFD software, the discretization of the geometry, and the probe lines used to collect the solution data.

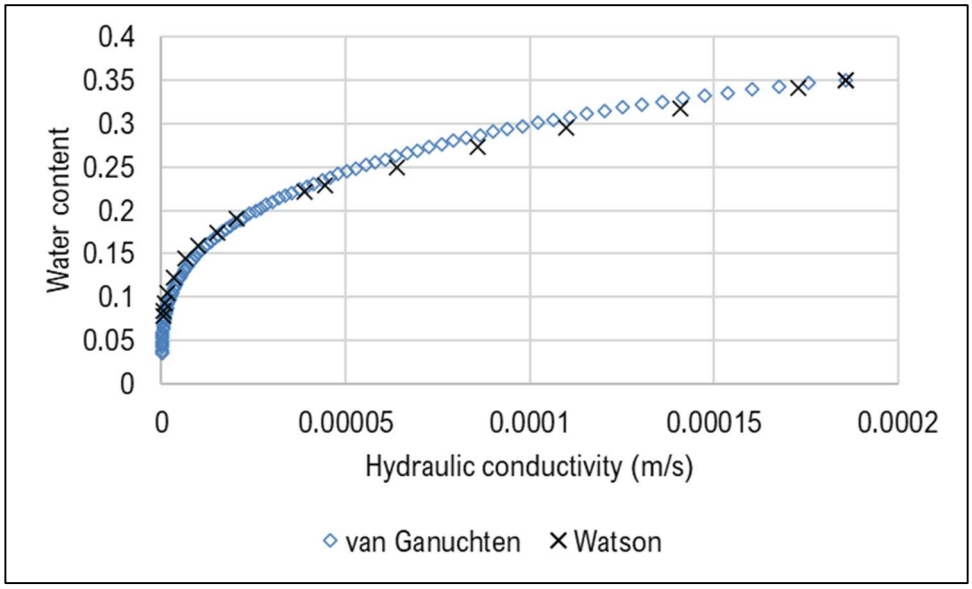



**Figure 3-3 Comparison of the experimental findings by Watson and van Genuchten model.**

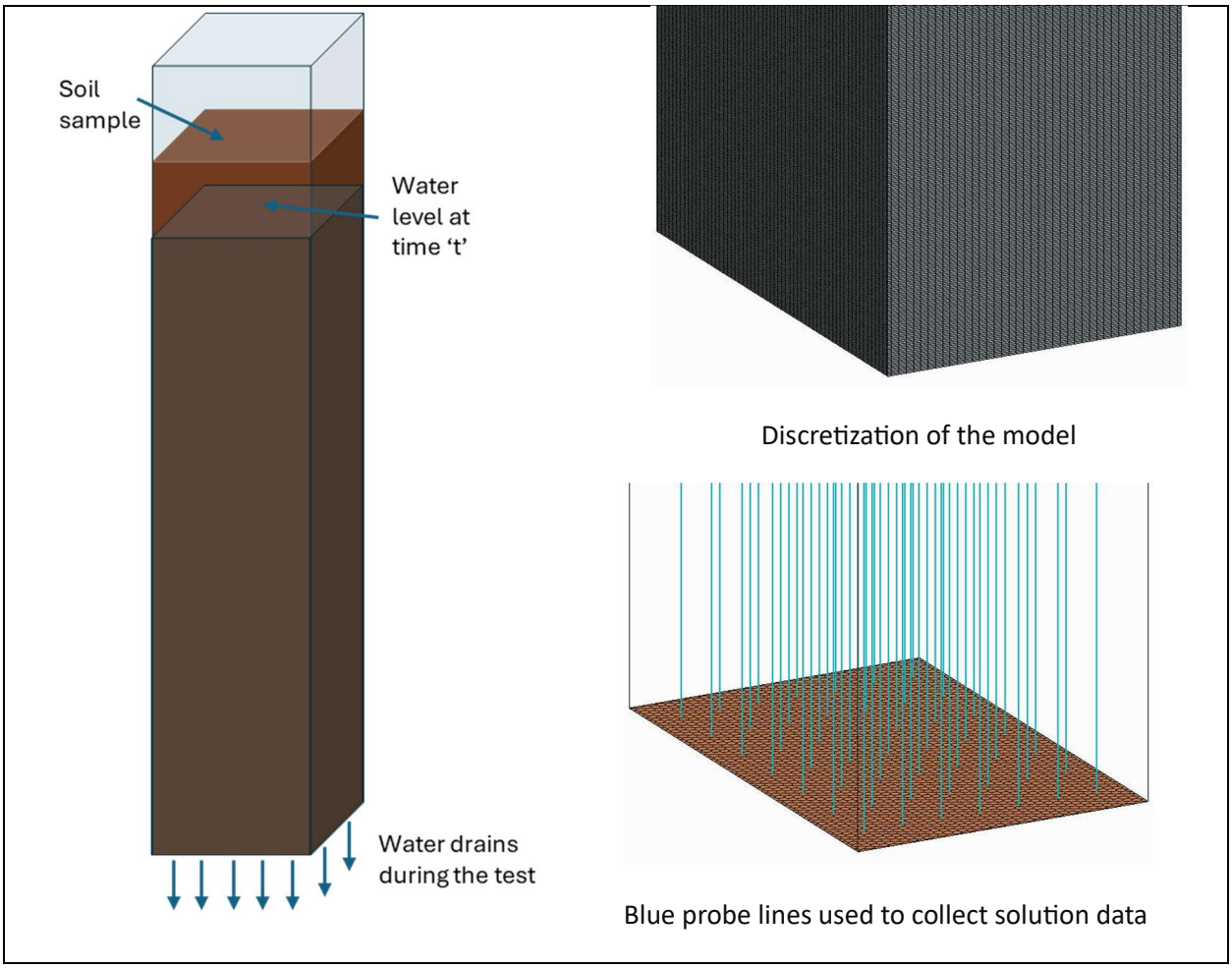



**Figure 3-4 Sketch of the soil sample and experimental set-up (left) and the discretization of the model and the lines used to record the solution (right).**

Figure 3-5 presents the vertical distributions of hydraulic conductivity and water content in the CFD model at 60 s of simulated drainage. The blue points correspond to values from individual computational cells intersected by the sampling lines, while the yellow points represent averages over 1 mm horizontal sections and therefore provide a clearer view of the mean vertical trend. The plotted vertical range was cropped to focus on the upper part of the sample, where drainage causes noticeable changes; below this region, both variables remain nearly constant. A visible scatter is present in cell-based data, particularly in the conductivity results, reflecting local cell-to-cell variability in the resolved flow field. The section-averaged values reduce this scatter and show that both hydraulic conductivity and water content decrease toward the top of the column as the soil drains and becomes progressively less saturated. In time, these profiles evolve as drainage progresses: the upper part of the column changes first and most strongly, and the zone of decreasing water content and conductivity gradually extends downward, indicating progressive decrease in saturation of the sample.

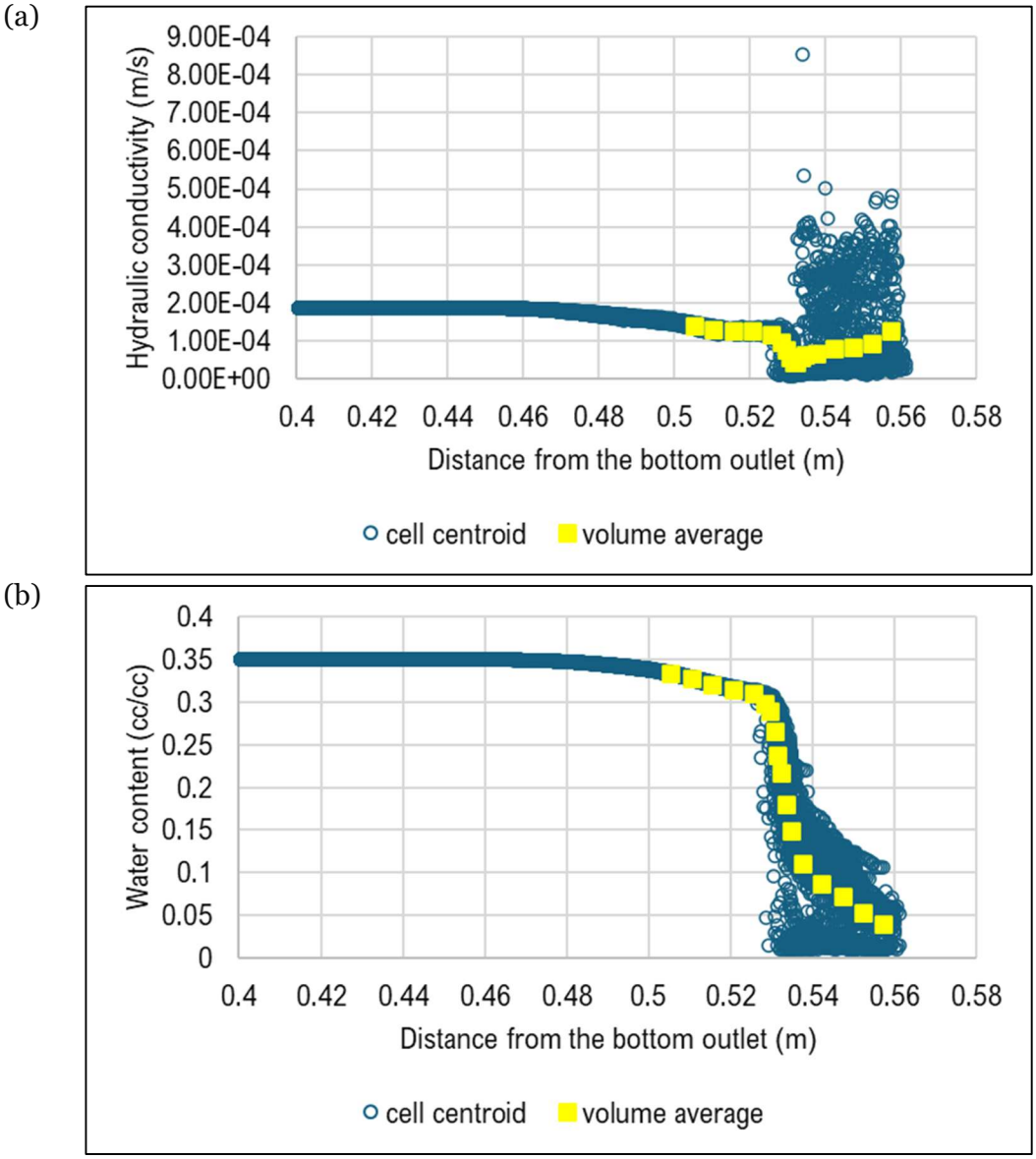



**Figure 3-5 Hydraulic conductivity (a) and water content (b) along the height of the CFD model at 60 seconds of simulated time.**

The results obtained with CFD models with the viscous resistance independent and dependent on the water content are presented in Figure 3-6 and Figure 3-7, respectively.

Figure 3-6 compares the hydraulic conductivity–water content relationship predicted by the CFD model with water-content-independent soil resistance against the experimental data reported by Watson. The CFD data were obtained by sampling values from computational cells intersected by a set of vertical lines uniformly distributed throughout the model domain, as illustrated in Figure 3-4, at multiple times during the drainage simulation. Thus, the plot combines point values extracted from different locations and different stages of drainage, allowing the evolution of the conductivity–water content relationship to be assessed over time. The results show substantial scatter, indicating both spatial and temporal variability in the cell-level response. Although the CFD predictions are comparable to the experimental results at saturation, corresponding to a water content of about 0.35 $m^3/m^3$, the model generally underestimates hydraulic conductivity at lower water contents. In addition, the predicted conductivity–water content relationship is not unique but varies with time, which suggests that a constant resistance formulation does not adequately capture the unsaturated flow behavior observed in the experiment.

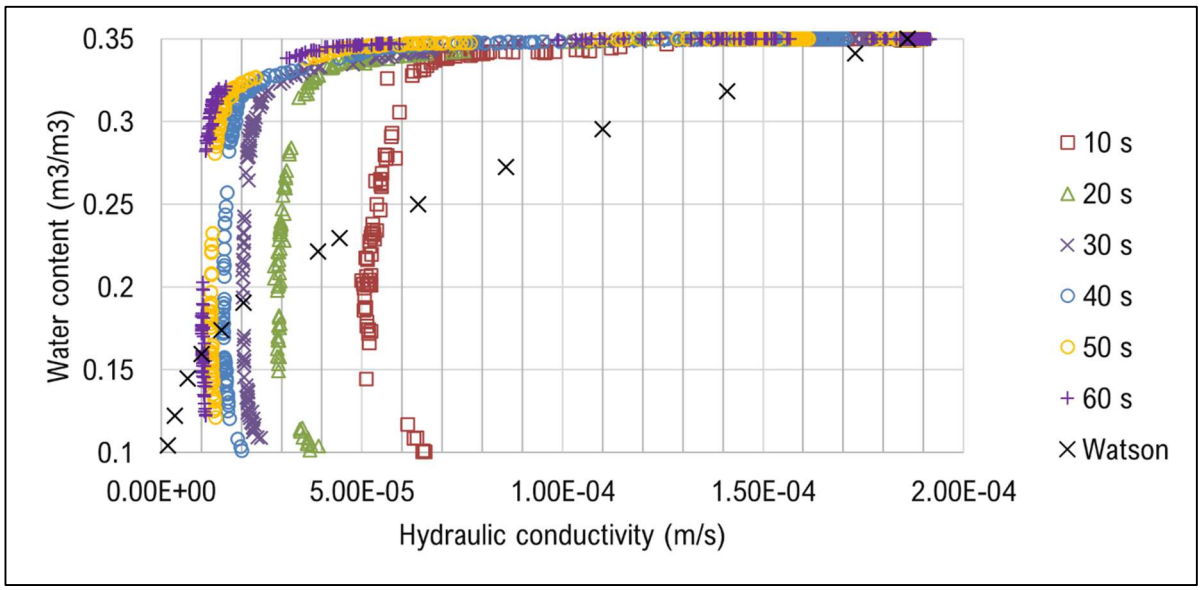



**Figure 3-6 CFD results from a model with flow-soil resistance independent of the water content compared with the experimental results by Watson.**

Figure 3-7 presents the hydraulic conductivity–water content relationship obtained from the CFD model with the van Genuchten formulation implemented to account for the dependence of soil flow resistance on water content, together with the experimental data reported by Watson. As in Figure 3-6, the CFD data points were extracted from cells intersected by vertical sampling lines uniformly distributed throughout the model domain at multiple times during the simulation, so the plot reflects both spatial and temporal variability during drainage. Although some scatter is still present, the results show a clearer and more consistent trend than the model with constant resistance. Overall, the predicted conductivity–water content relationship agrees more closely with Watson's measurements, indicating that incorporating water-content-dependent resistance provides a more realistic representation of unsaturated flow behavior in the sand column.

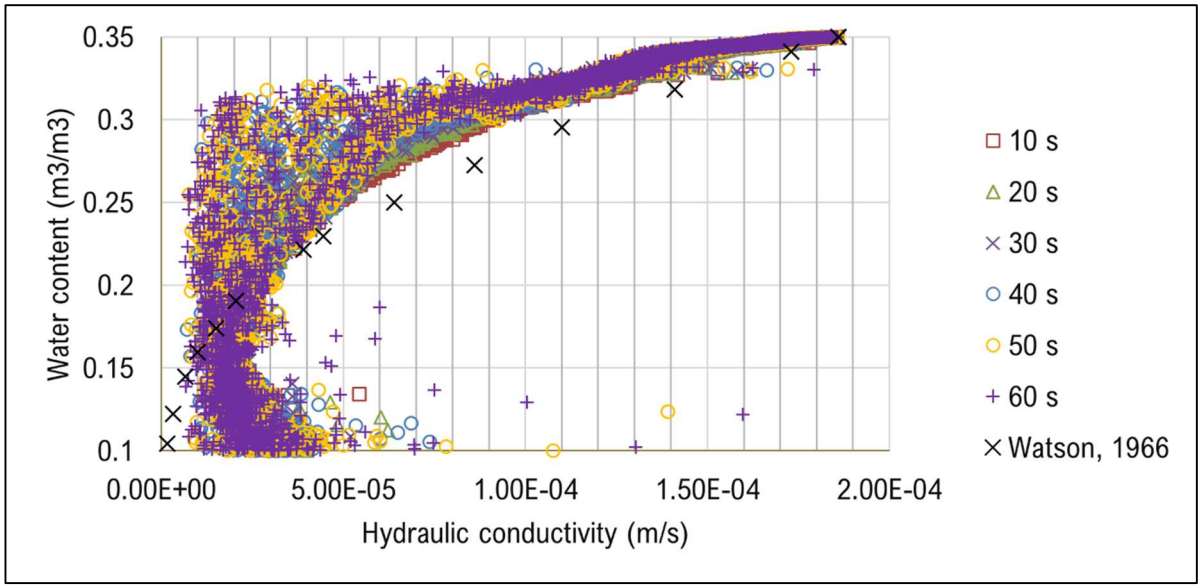



**Figure 3-7 CFD results from a model with implemented van Genuchten model of water flow in unsaturated soils compared with the experimental results by Watson.**

Figure 3-8 compares the hydraulic conductivity–water content relationship at 60 s of simulated time obtained from the CFD model with variable conductivity and from the VS2D model against Watson's experimental data. Unlike Figure 3-6 and Figure 3-7, which combine data from multiple times during the simulation, Figure 3-8 shows results at a single selected time, allowing a more direct comparison of the model predictions at that stage of drainage. Both computational approaches reproduce the experimental trend reasonably well for water contents above approximately 0.2 $m^3/m^3$. At lower water contents, however, the CFD model tends to overestimate hydraulic conductivity, while the VS2D results do not extend below about 0.24 $m^3/m^3$. The figure therefore shows that the variable-conductivity CFD model captures the unsaturated behavior relatively well over the intermediate moisture range, but discrepancies remain in the drier portion of the domain.

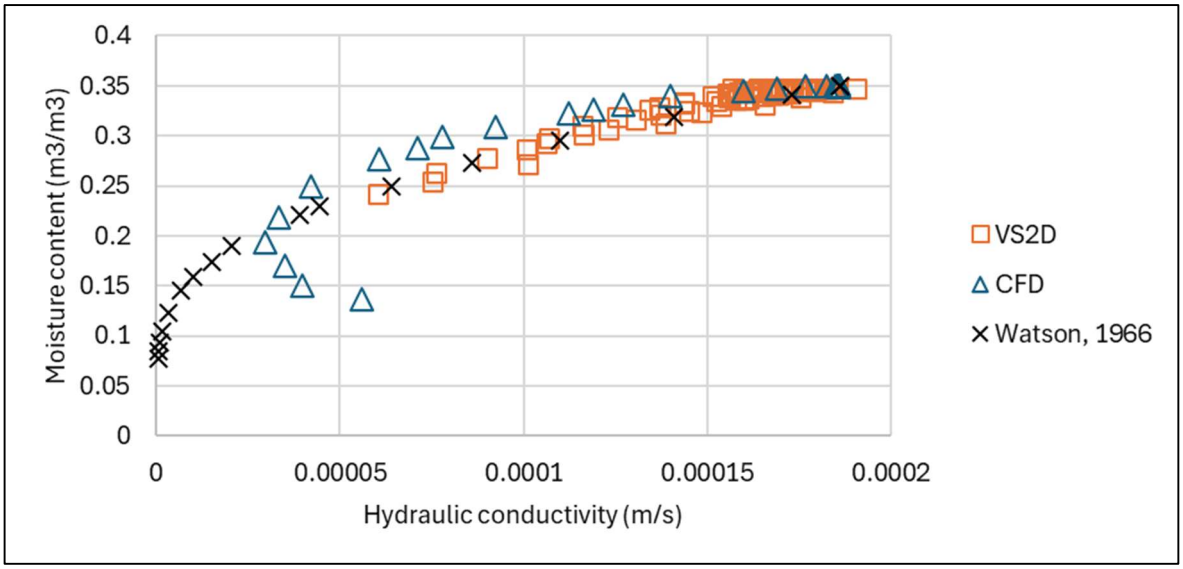



**Figure 3-8 Water content vs. hydraulic conductivity at 60 seconds of simulated time for the CFD model with variable conductivity and VS2D model compared to Watson's results.**

### 3.2.2 Verification Example: Jurin's Law

Capillary rise is the upward movement of water between soil particles due to a combination of the cohesion and adhesive forces between water and particle surfaces. In fine soil, the upward movement of water is slow but covers a long distance. On the other hand, in coarse soil, the upward movement of water is quick, but covers only a short distance.

An experimental set-up used in laboratories to study fluid properties such as viscosity and surface tension involves an empty capillary tube whose lower end is immersed in water was used as a reference case with a known solution to check CFD capabilities. During the experiment, a concave free surface forms inside the tube. Depending on its inner diameter, water rises to a different height. Water rises due to the adhesion forces between water and the solid, until the forces are balanced by the gravity force. Jurin's law [23] is commonly used to calculate the height of water rise in a capillary tube:

$$h = \frac{2\sigma \cos\theta}{\rho g r} \tag{3.12}$$

where: $\sigma$ is surface tension, $\sigma = 0.072$ N/m, $\theta$ is contact angle, $\theta = 60$ deg for water, $\rho$ is liquid density, $\rho = 998$ kg/m$^3$, $g$ is gravity acceleration, $g = 9.81$ m/s, and $r$ is tube radius, $r = 0.25$ mm.

The results of the computations are presented in Figure 3-9. On the left side, the figure shows the final water level in the tube, a close-up view of the meniscus, and on the right side, the plot of water level vs. simulated time compared with the capillary rise calculated using equation (3.12). The computational solution is comparable with the hand calculations as CFD converges to 29.07 mm, and Jurin's law gives 29.42 mm of capillary rise.

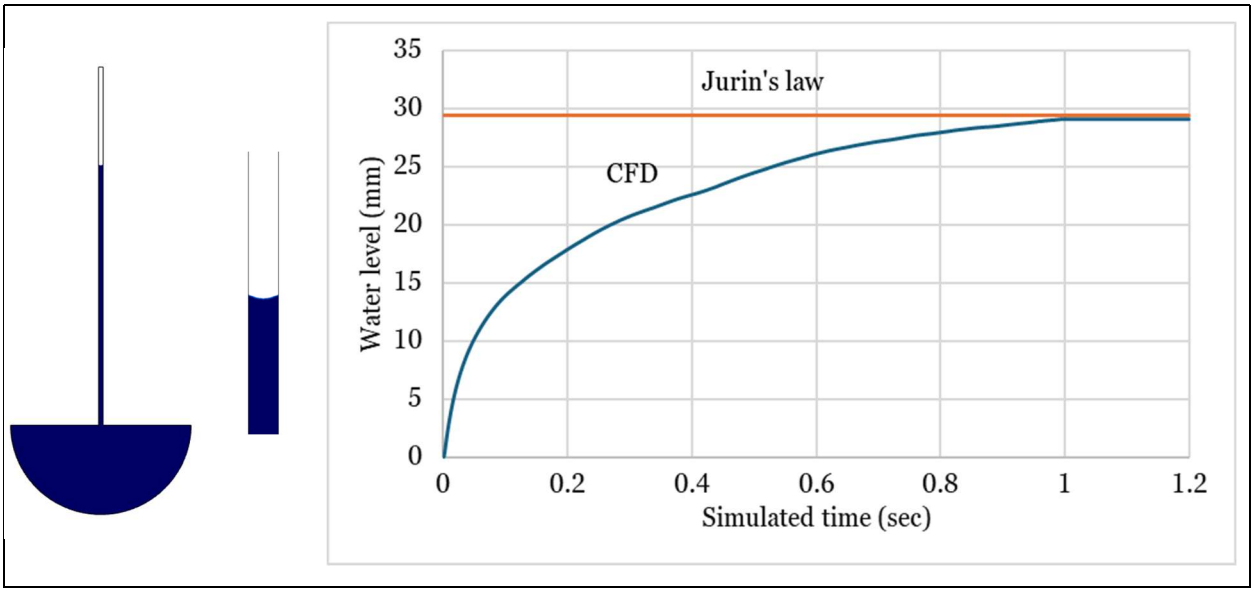



**Figure 3-9 Capillary rise of water in a tube. The water level at the end of the simulation, a close-up view of the meniscus, and a plot of the rise of water level in time compared to the Jurin's law.**

The capillary rise can be represented using the surface tension model only when the fluid moves between wall boundaries, like the walls of a tube. If this approach is to be used to model capillary rise in soil, then the space between the separate sediment grains needs to be meshed out and the

grains' surfaces should be wall boundaries. Meshing soil void space would lead to hundreds of millions of volume cells, which is not feasible with the available computer resources.

An alternative approach to model the capillary rise in porous media was found in [24], where the tube radius is replaced in equation (3.12) with an "effective radius"

$$r_{eff} = \frac{2(1-\phi)}{\phi\rho\bar{A}} \tag{3.13}$$

where $\phi$ is solid volume fraction, $\rho$ is solid density, $\bar{A}$ is specific surface area of the solid fraction. Assuming that the grain shape is close to spherical, the specific surface is calculated from $\bar{A} = 6/(\rho d_{50})$. For the water surface rise to be $h$, the pressure applied to the water surface should be

$$p = \rho g h = \frac{6\phi\sigma\cos\theta}{(1-\phi)d_{50}} \tag{3.14}$$

However, it is much simpler to apply this pressure to the outlet boundary at the top of the tube and ignore the relatively small pressure drop in the column of air above the water surface.

Figure 3-10 presents a CFD model of a short pipe and aspherical volume underneath it, filled with porous media. The saturated hydraulic conductivity is 0.004, porosity is 0.35, which results in mean grain diameter 0.73 mm. At time zero, the empty space is filled with water, and the tube is filled with air. The boundary conditions marked with grey are no-slip walls, and with orange are pressure outlets. The pressure assigned at the surface of the half-sphere is hydrostatic pressure. At the top of the tube, a negative (pointing upwards) pressure calculated with equation (3.14), is applied. During the simulation, the water surface moves upward up to 0.111 m. Jurin's law gives 0.112 m.

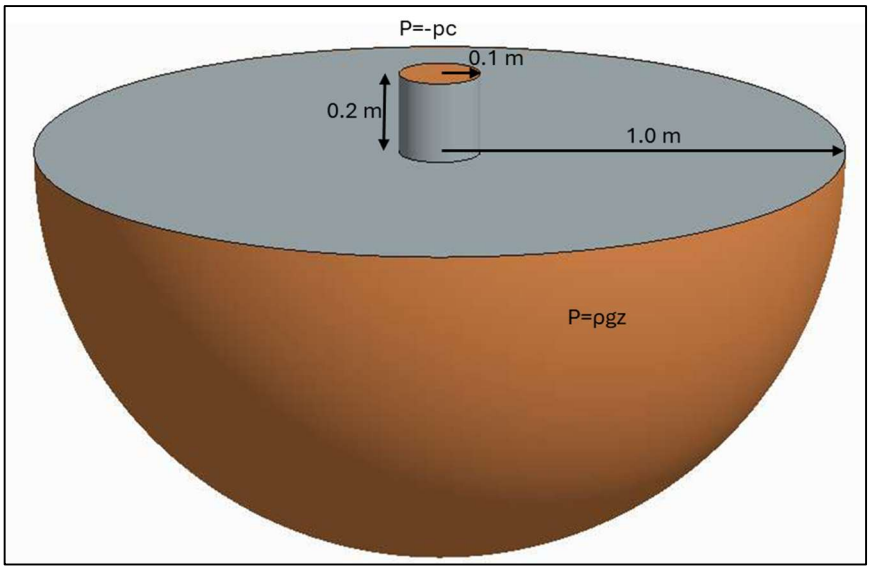



**Figure 3-10 Model used to analyze the capillary rise in porous media.**

Figure 3-11 shows a contour plot of the volume fraction of water in the tube at the end of the simulation, and a point plot along the centerline with highlighted location of the water surface

(water VOF=0.5) above which the soil is not fully saturated. The shape of the curve compares well with similar results reported in literature [25]

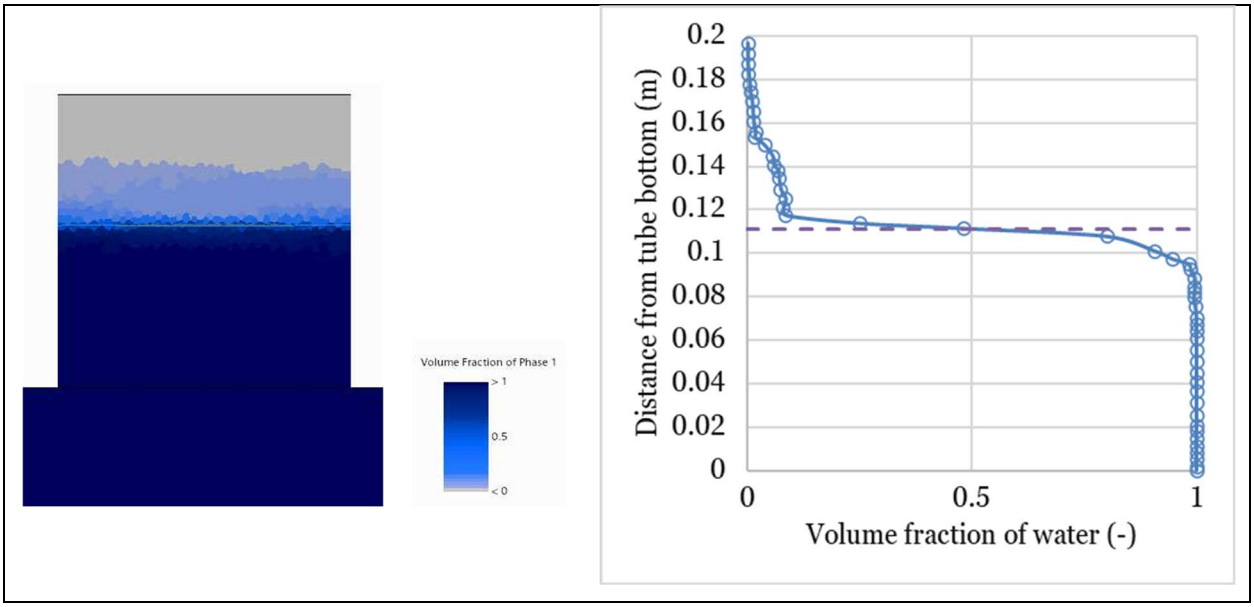



**Figure 3-11 Volume fraction of water in a tube filled with porous medium at steady state, left- contour plot on a plane section through the computational domain, right- point plot along the tube centerline.**

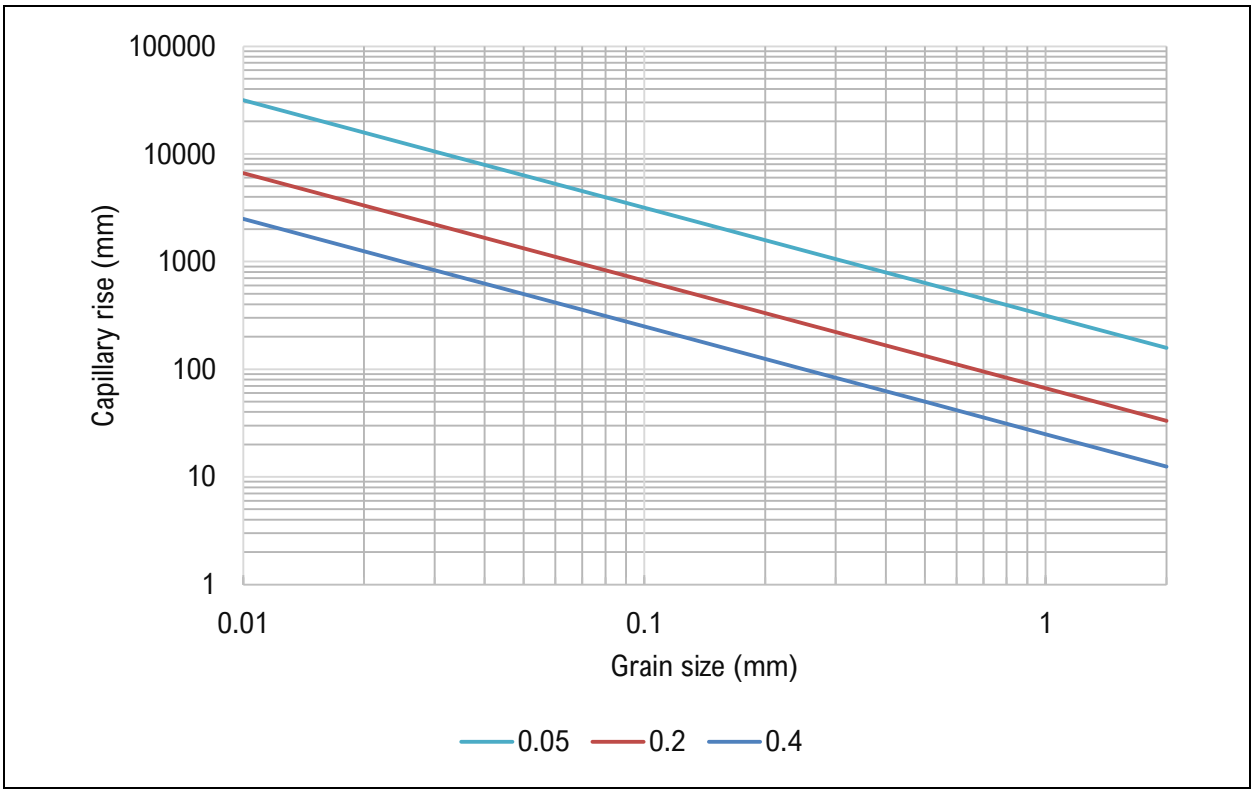



**Figure 3-12 Capillary rise dependence on grain size and soil porosity.**

Figure 3-12 presents the capillary rise dependence on grain size for soil porosity 5%, 20% and 40% calculated using equation (3.14). The curves are plotted on a log-log scale. The rise increases with decreasing grain size in the range from a few inches to a few yards. Table 3-2 shows results for a set of conditions.

**Table 3-2 Capillary rise in porous media.**

| | **h (in)** | | |
|---|---|---|---|
| **porosity (-)** / **d (mm)** | **0.4** | **0.2** | **0.05** |
| 0.01 | 98.14 | 261.69 | 1243.05 |
| 0.1 | 9.81 | 26.17 | 124.31 |
| 1 | 0.98 | 2.62 | 12.43 |

# 4 Ditch-Embankment Infiltration Predictions

The computational modeling starts with a base case, in which the embankment is built of sandy soil with zero initial moisture, porosity of 0.4 and grain diameter of 0.2 mm. The horizontal distance between the edge of the subbase and water free surface edge is 10 ft, comprised of a 4 ft shoulder at 12.5:1 slope and 6 ft 8 in of a ditch with front slope 4:1. The combined pavement and subgrade is one foot deep. The ditch is fully filled with water, which means that the freeboard is negative. The discretization of the CFD models with a refinement at the border between regions of different porosity are presented in Figure 4-2.

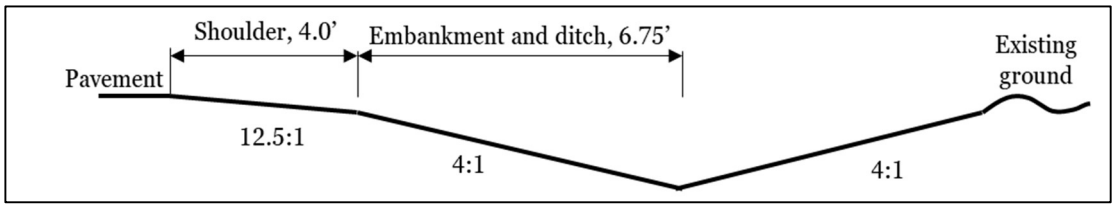



**Figure 4-1 Geometry of the base case model.**

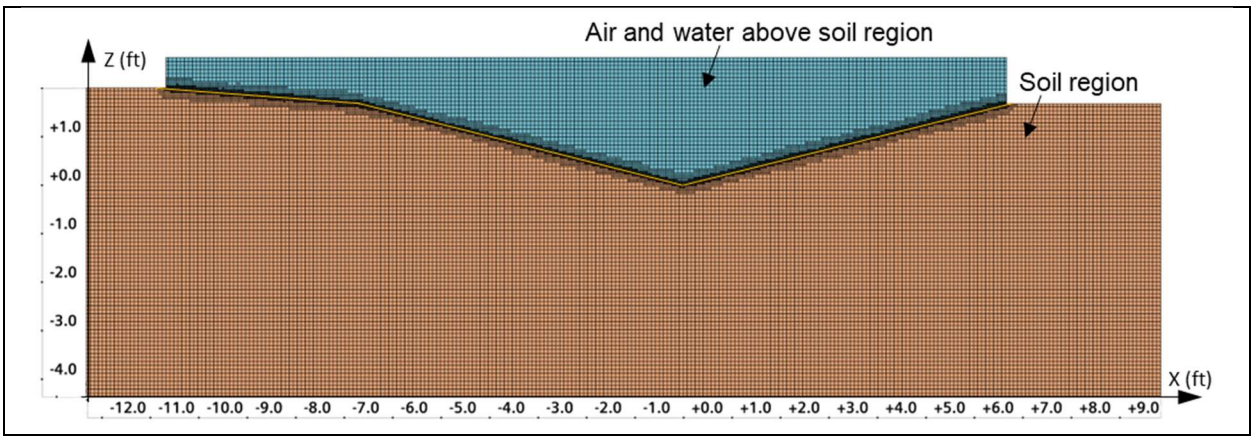



**Figure 4-2 Discretization of an example CFD model with a refinement at the border between regions of different porosity.**

At the beginning of the simulation, the ditch is filled with water, and the rest of the volume is filled with air. During the simulation water infiltrates into the porous region, leaving the ditch. A volumetric source term is used to keep the water level constant replacing water that leaves the ditch, which covers the effects of replacement by rain and drainage of water into the ditch from the surroundings. Figure 4-3 shows the volume fraction of water and velocity vector field at 60 seconds of simulated time in the domain. The water saturation is plotted as a surface in shades of blue, with the lightest shade signifying the lowest water content, and the darkest shade signifying a 100% saturation. The vector field plotted in the figures shows the direction and magnitude of the air-water mixture velocity. The range of values was cropped to eliminate local peaks in the air above the water surface and possible imperfections in the mesh (which do not have impact on the overall solution). The velocity vectors show a close to symmetric air-water mixture movement in the soil with the centerline going through the bottom of the ditch. The spatial distribution of the direction is non-uniform and depends on the moisture content; the downward direction prevails in water close to the centerline; when moving away from the centerline, the direction changes to horizontal and finally to an upward direction. By comparing Figure 4-3, Figure 4-4, and Figure 4-5 one can observe the progression of the infiltration into the soil under the ditch over 20 minutes of simulated time. By that point, the maximum horizontal extent of the waterfront moved past the embankment and the risk of seepage into the subbase is gone.

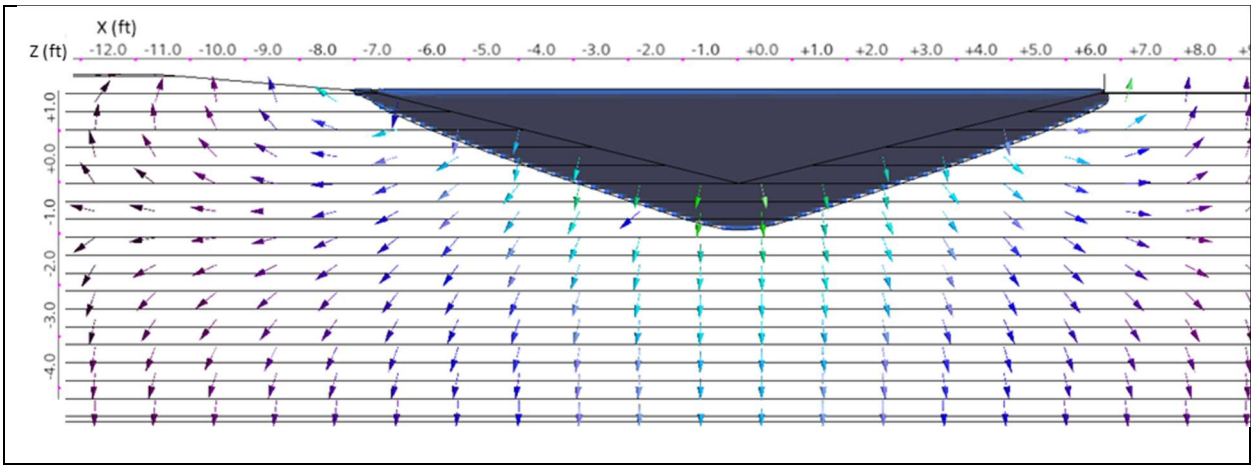



**Figure 4-3 Volume fraction of water in the base case at 1 minute of simulated time.**

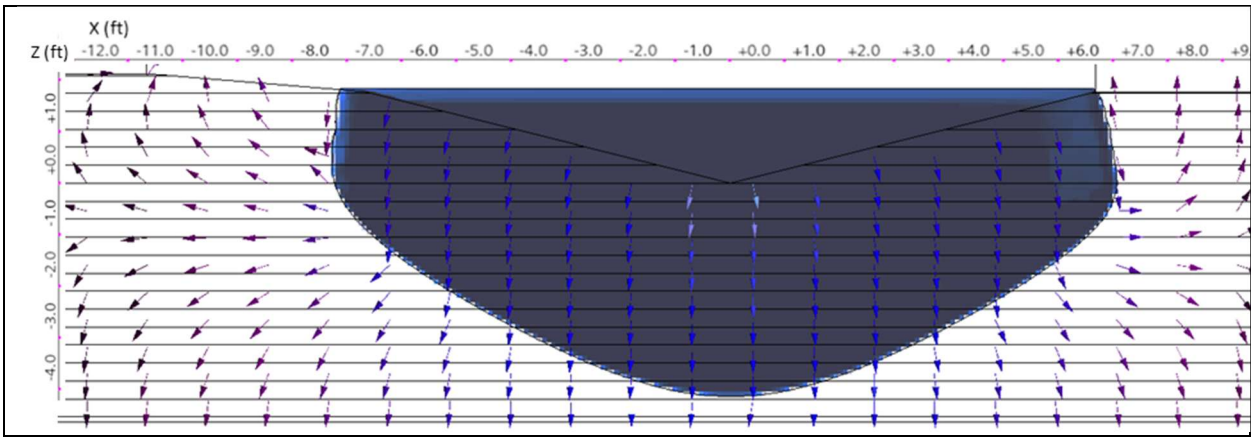



**Figure 4-4 Volume fraction of water in the base case at 10 minutes of simulated time.**

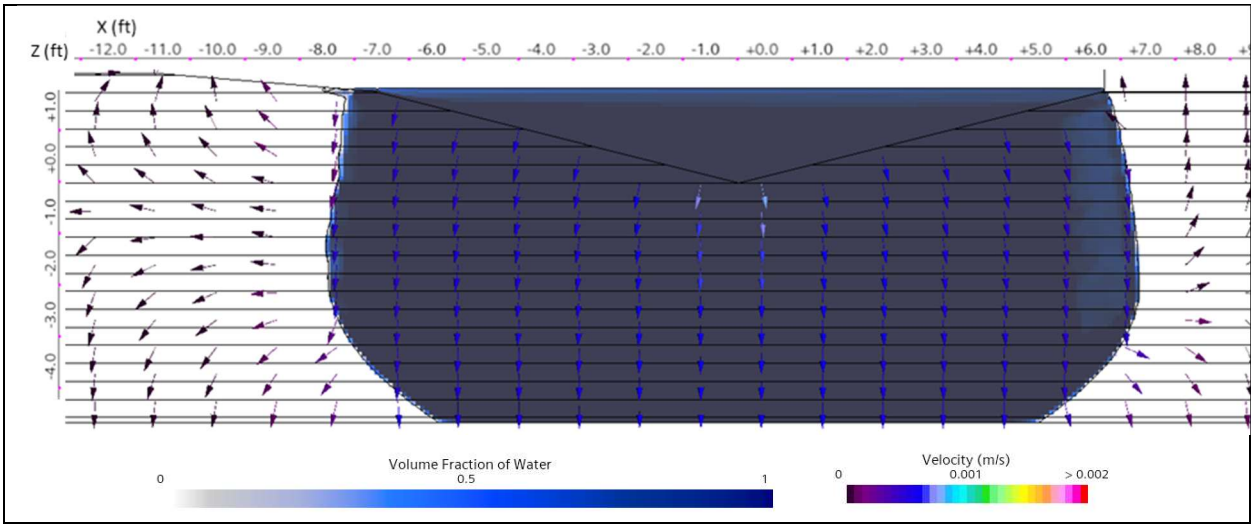



**Figure 4-5 Volume fraction of water in the base case at 20 minutes of simulated time.**

## 4.1 Impact of Capillary Pressure

The base case was modified to add the model of capillary pressure as described in Section 3.2.2. The top surface of the embankment was changed from an interface between regions of different porosity to a pressure outlet boundary with $p = -p_c \cos(1/12.5)$. Also, the gauge pressure on the horizontal surface on the right side of the ditch was changed from zero to $p = -p_c$. The difference in the shape of the waterfront can be seen in Figure 4-6 and Figure 4-7 where the base case (a) is compared to the modified model (b) at one minute and ten minutes of simulated time. Due to the added negative pressure on the ground surface, the groundwater spreads more sideways as compared to the default case, but the main flow direction remains to be downwards, which is represented by the direction of the velocity vectors. Despite the increased horizontal extent of the infiltration, the ditch frontside and shoulder are wide enough that the water does not reach the subbase. Figure 4-8 shows the progress of the infiltration after 20 minutes of simulated time. By then, the point of maximum horizontal extent is already lower than the bottom of the subbase.

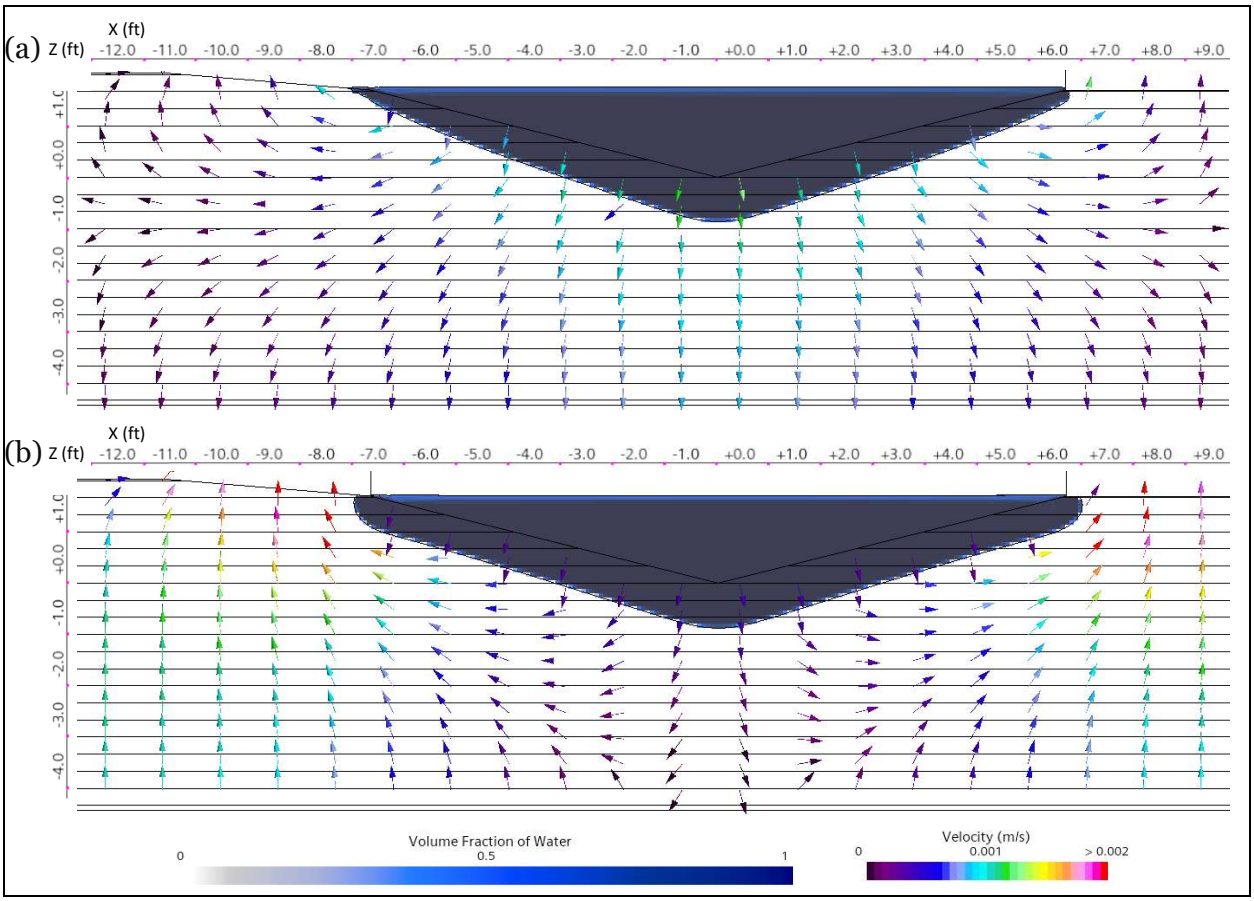



**Figure 4-6 Comparison of the extent of infiltration within a minute of simulated time in the model (a) without and (b) with capillary pressure.**

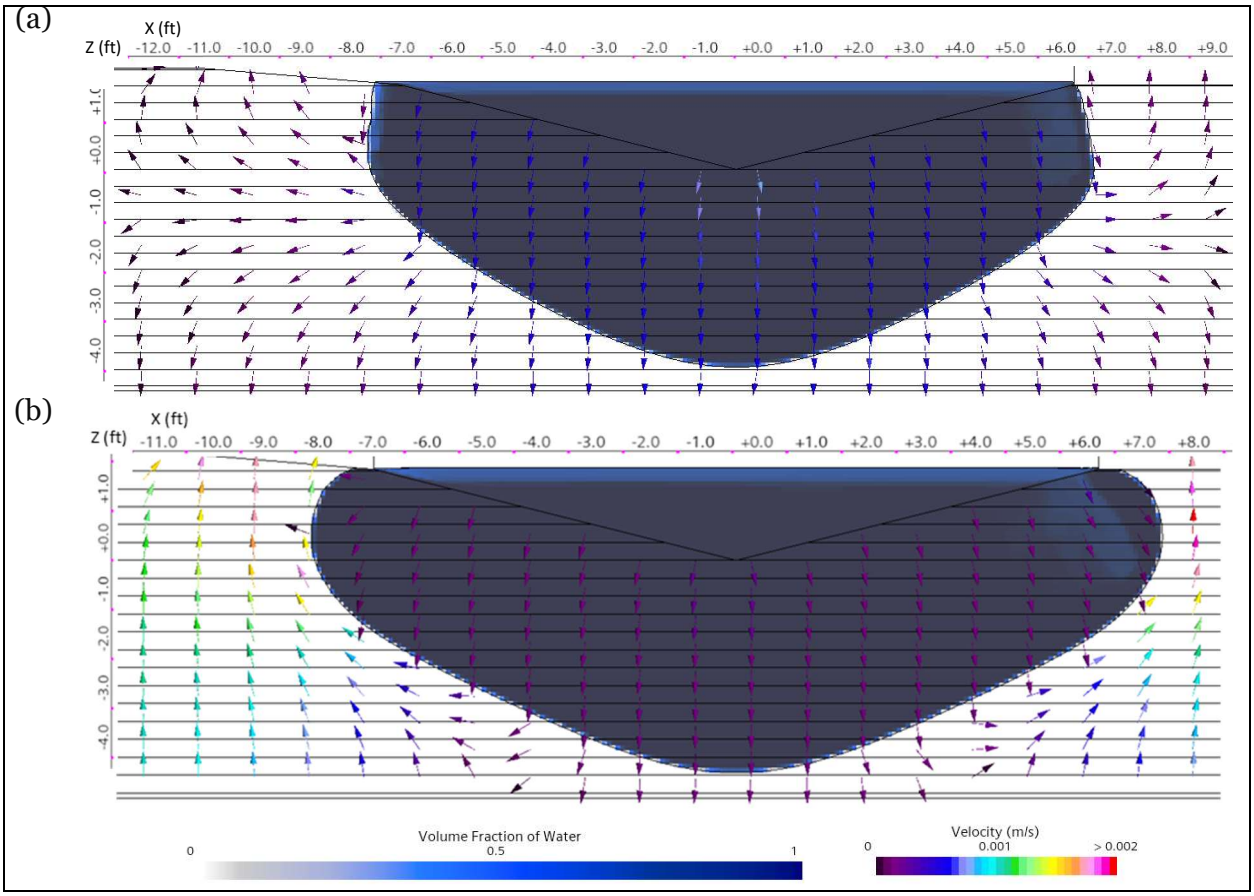



**Figure 4-7 Comparison of the extent of infiltration within 10 minutes of simulated time in the model (a) without and (b) with capillary pressure.**

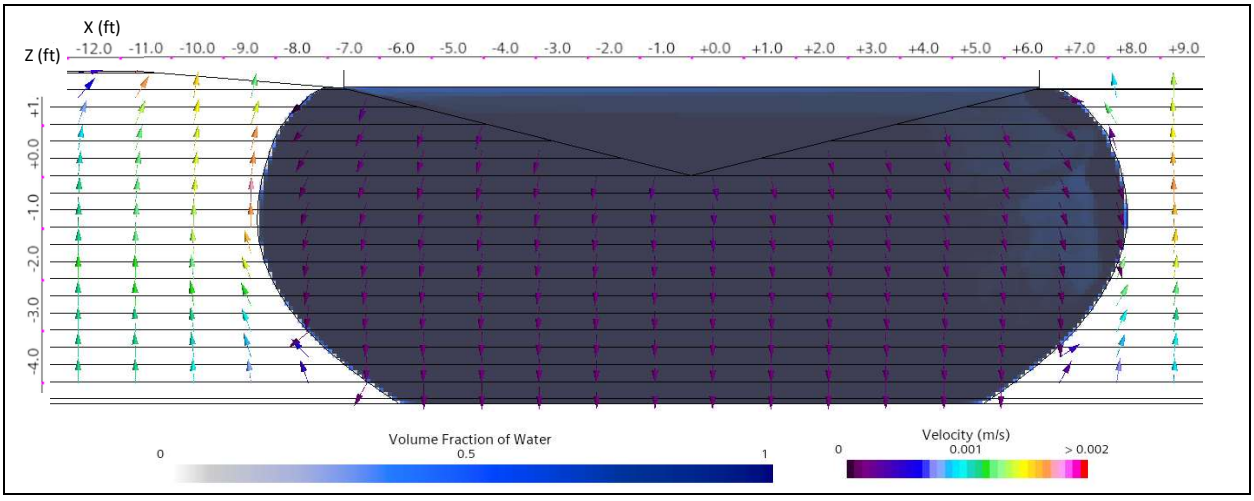



**Figure 4-8 Progress of the infiltration in the model with capillary pressure after 20 minutes of simulated time.**

## 4.2 Impact of Soil Porosity

The impact of the porosity on the infiltration was analyzed based on grain sizes 0.01 mm and 2.0 mm. The porosity varies from 5% to 40%. The difference for the two grain sizes is noticeable in Figure 4-9 which shows screenshots of the water content in the ditch and soil at 1 hr of simulated time. The infiltration into the soil made of the smaller grains is insignificant as the water infiltrates only up to a couple of inches into the embankment during this time. If the soil is made of 2-mm particles, the groundwater movement is faster, and it increases with increasing porosity. The downward movement prevails over horizontal movement, with the horizontal velocity component decreasing when the porosity increases. The water content colored in shades of blue in the figure also illustrates this; the horizontal extent of the fully saturated soil is similar and the water content in the unsaturated soil decreases. None of the scenarios result in ground water reaching the subbase.

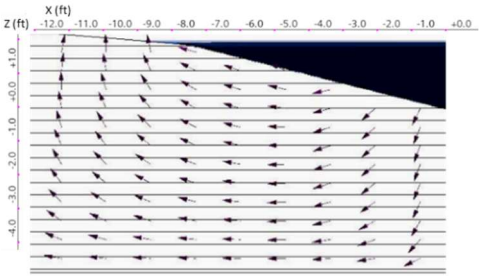
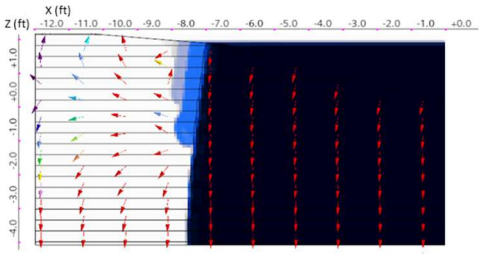
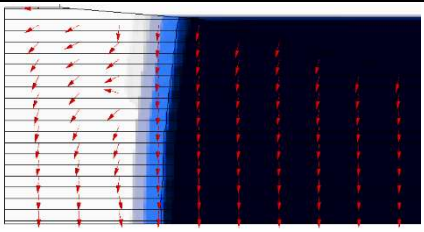
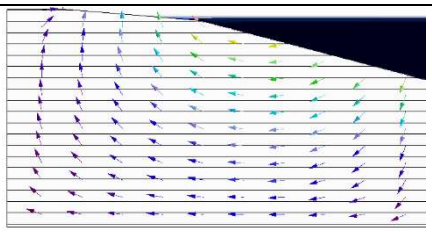
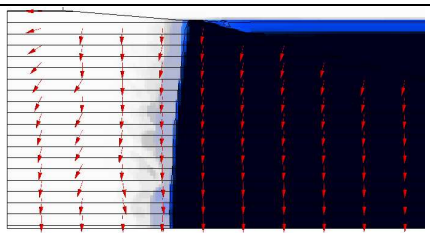
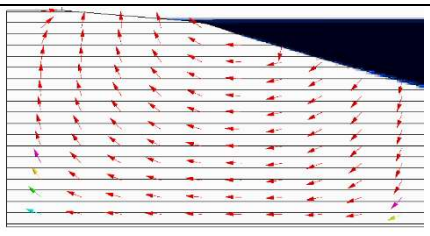
| Porosity | Grain size 0.01 mm | Grain size 2.0 mm |
|---|---|---|
| 0.05 |  |  |
| 0.1 | n.a. |  |
| 0.2 |  |  |
| 0.4 |  | n.a. |
| |  | |

**Figure 4-9 Impact of soil porosity on the infiltration extent.**

## 4.3 Impact of Grain Size

An hour-long rain event was considered, during which the ditch is fully filled with water. The soil is compacted to 95%. Figure 4-10 shows the infiltration extent at 1 hour of simulated time for soils with varying grain sizes, from 0.001 mm to 2 mm. The extent of the infiltration is insignificant for the grain size less than a millimeter. For grain sizes >1 mm, the maximum vertical spread differs (increases with the grain size), and the horizontal spread is similar, at about 0.2-0.3 m (0.7-1 ft).

| Grain size | Infiltration extent |
|---|---|
| 0.001 mm | |
| 0.01 mm | |
| 0.1 mm | |
| 1.0 mm | |
| 2.0 mm | |

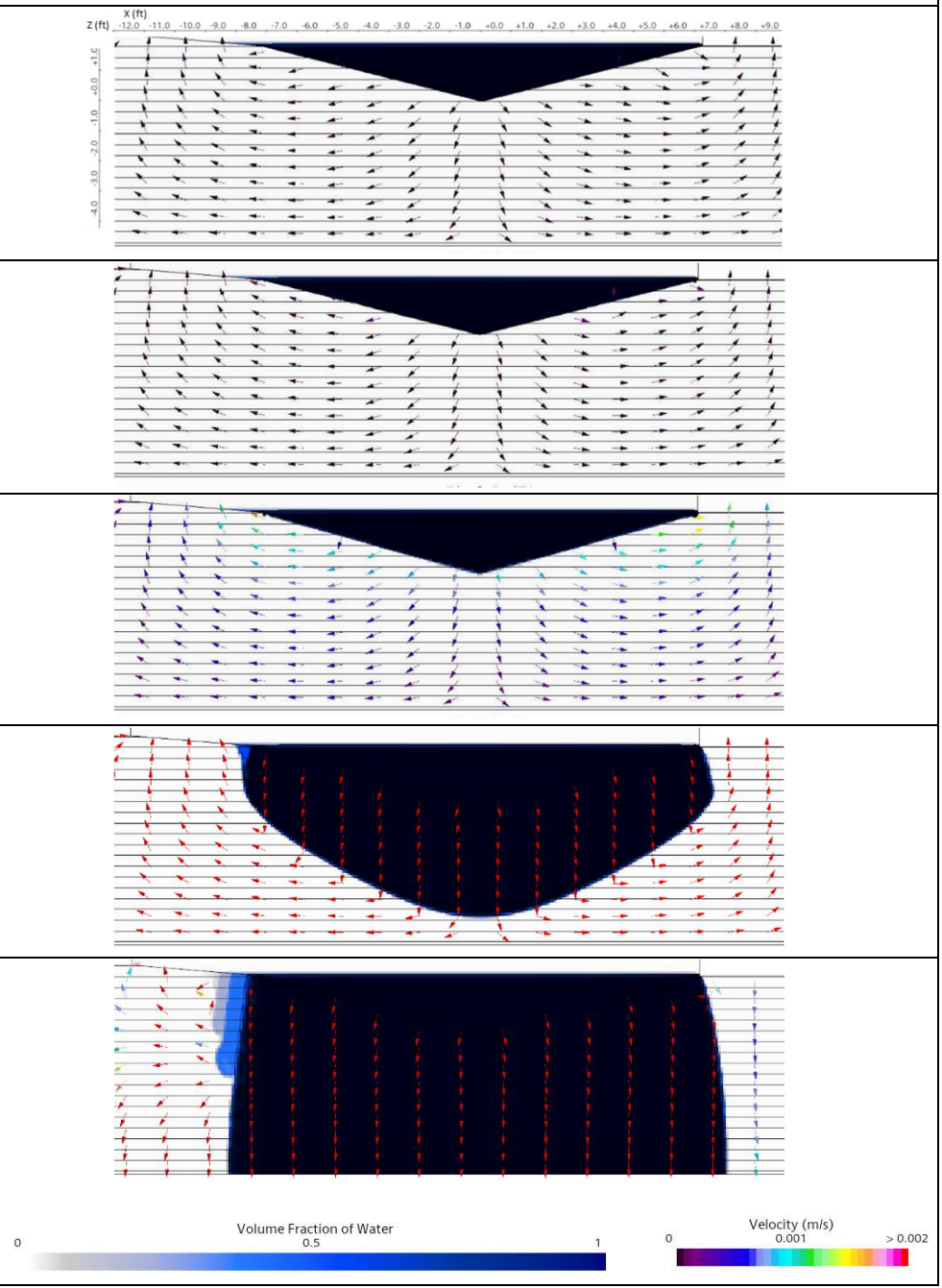



**Figure 4-10 Water infiltration at 1hr of simulated time. Soil compaction is 95%, grain size varies.**

Figure 4-11 shows a close-up view of the top edge of the ditch for two selected grain sizes, 0.1 and 1.0 mm. The difference in the infiltration extent within the same time is significant. However, the horizontal extent is still small at the largest grain size.

Figure 4-12 shows the extent of the infiltration into soil with grain size 1 mm, porosity 5% and no initial moisture content at various times during the simulation. It can be observed that even though the horizontal water movement progresses with time, the vertical downward movement prevails. Therefore, the waterfront does not reach the subbase within the considered time span.

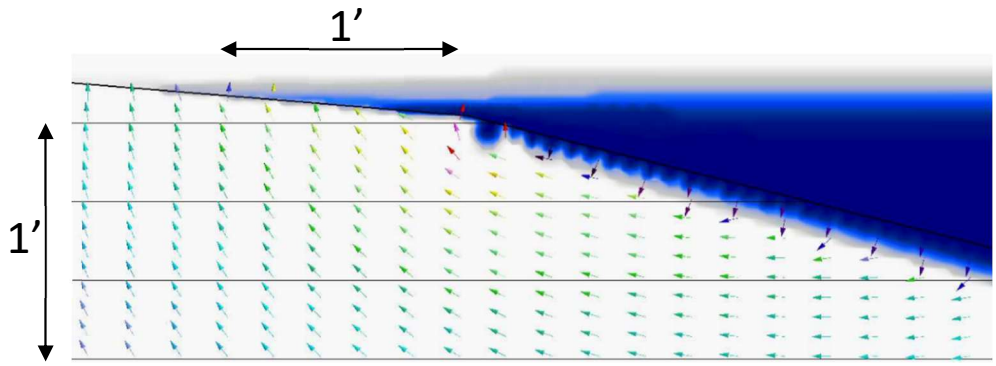
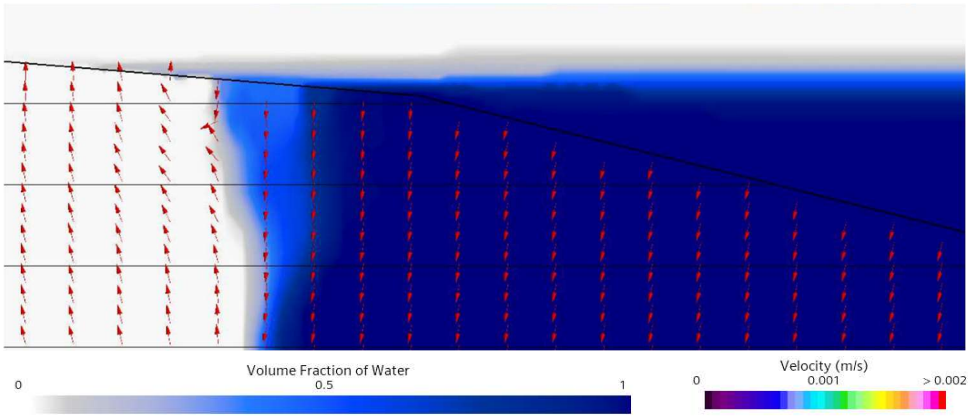
| Grain size | Infiltration extent |
|---|---|
| 0.1 mm |  |
| 1 mm |  |

**Figure 4-11 Close-up view of the infiltration near the top edge of the ditch.**

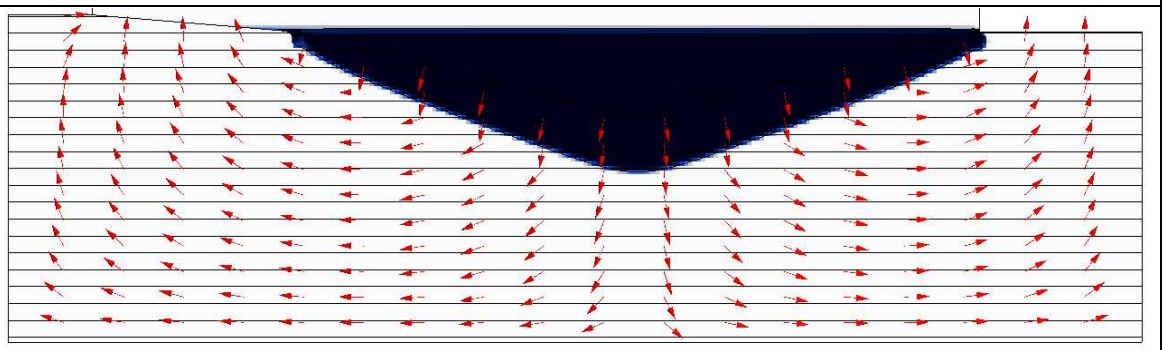
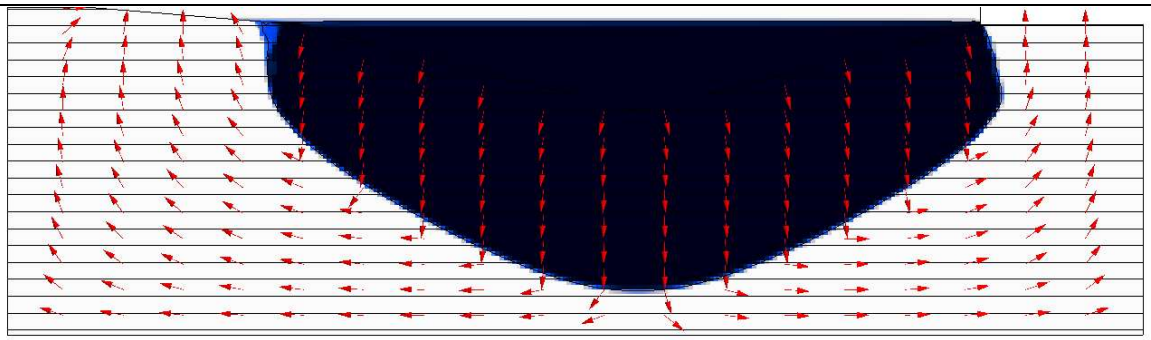
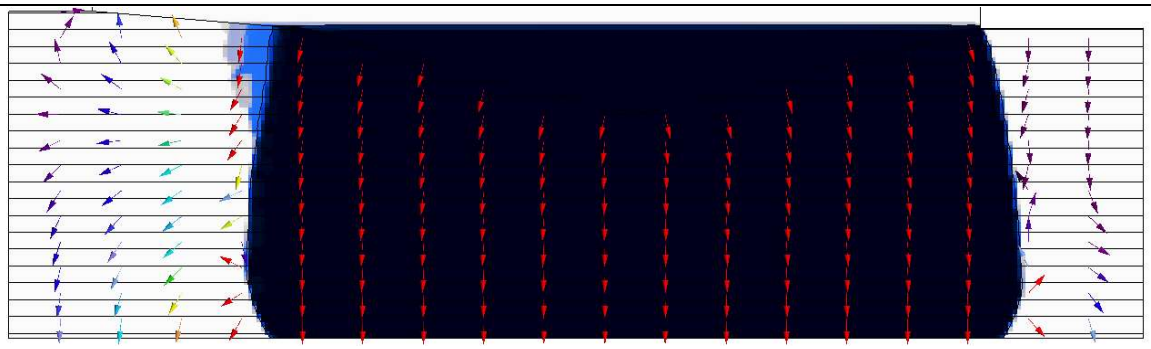
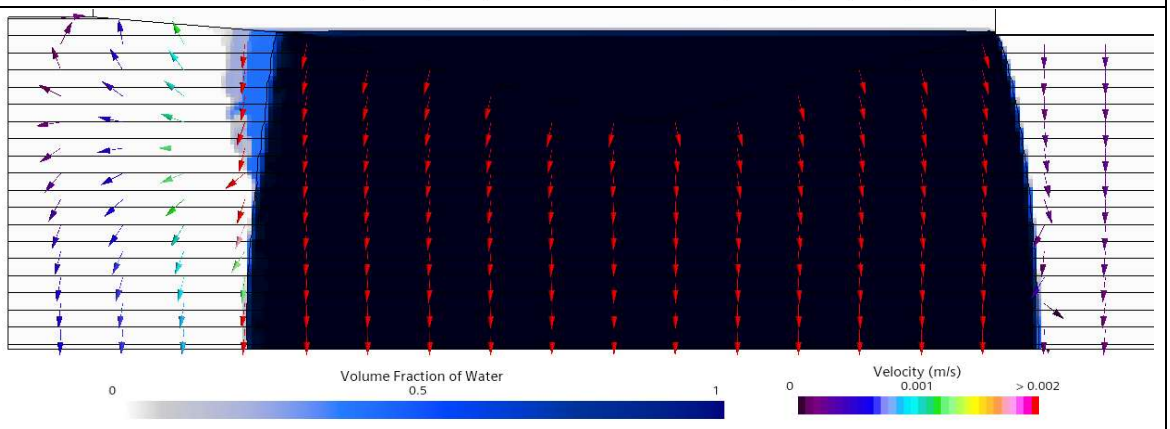
| Time | Infiltration extent |
|---|---|
| 600 s |  |
| 1 hr |  |
| 3 hr |  |
| 4 hr |   |

**Figure 4-12 Infiltration at various times for soil grain size 1 mm and porosity 5%.**

## 4.4 Impact of Initial Moisture Content

The impact of initial soil moisture on infiltration is shown by comparing dry soil with soils whose pores are initially 15% and 30% filled with water. Differences among cases are indicated by color variations—from white to darker blue—outside the saturated zone. Higher initial moisture content slows infiltration from the ditch. In addition, the water–air interface, which is relatively smooth when the pores initially contain only air, becomes distorted and highly irregular as initial moisture increases. Figure 4-13 shows the water content at 1 hour of simulated time.

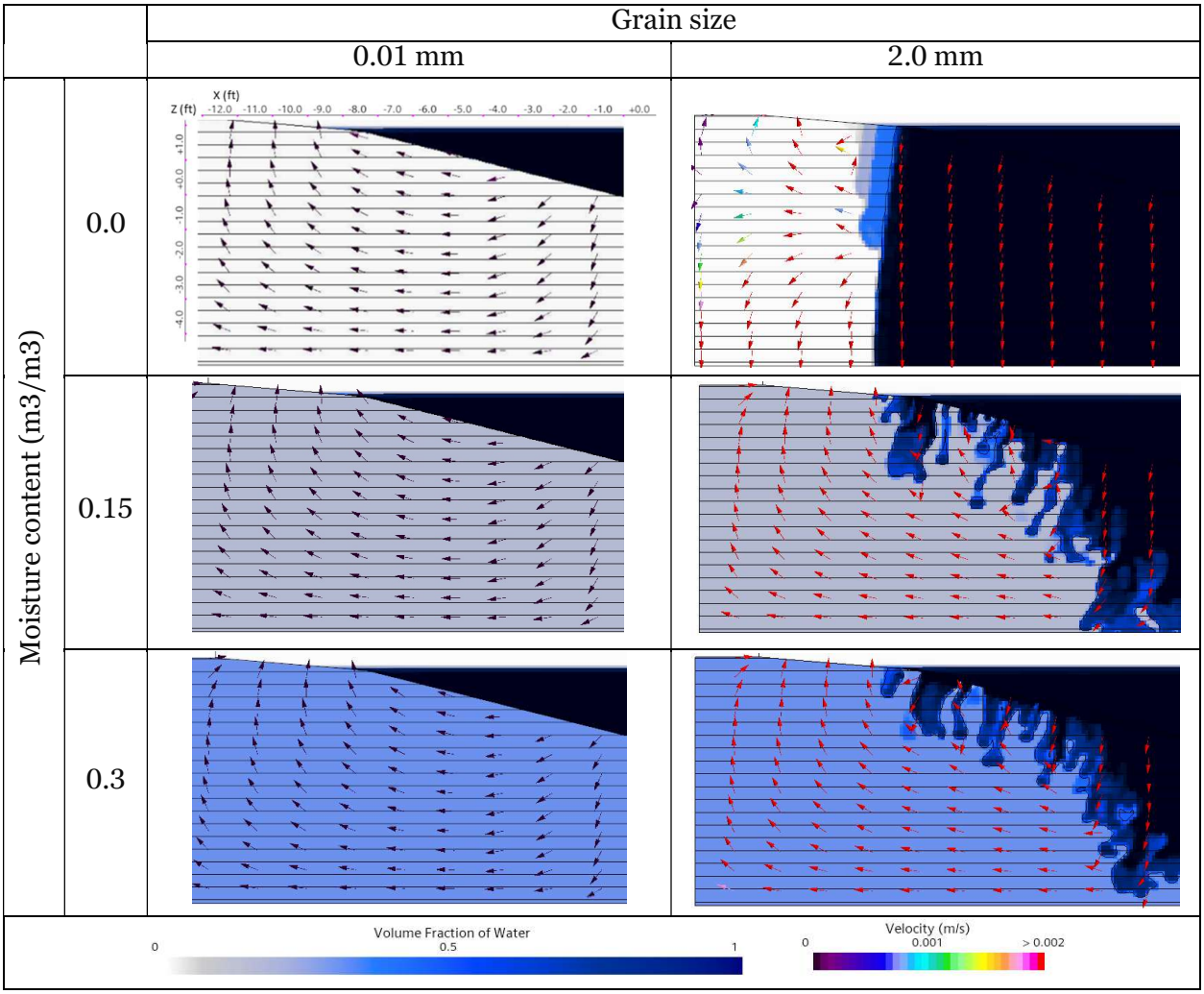



**Figure 4-13 Impact of initial soil moisture content on water inflitration.**

## 4.5 Impact of Groundwater

The presence of groundwater was simulated by initiating the simulation with the volume fraction of water equal to one in the soil volume up to the bottom of the ditch and up to one foot below the bottom. The initial groundwater level is marked with dashed green line. The side and bottom surfaces of the domain are walls instead of outlets so that the water level does not drop during the simulation. The water level may only increase due to the infiltration from the ditch. Two grain sizes, 0.25 mm and 2 mm, and two porosities, 0.05 and 0.4 were tested. Water surface in the ditch is at the same level as the bottom of the subbase (zero freeboard).

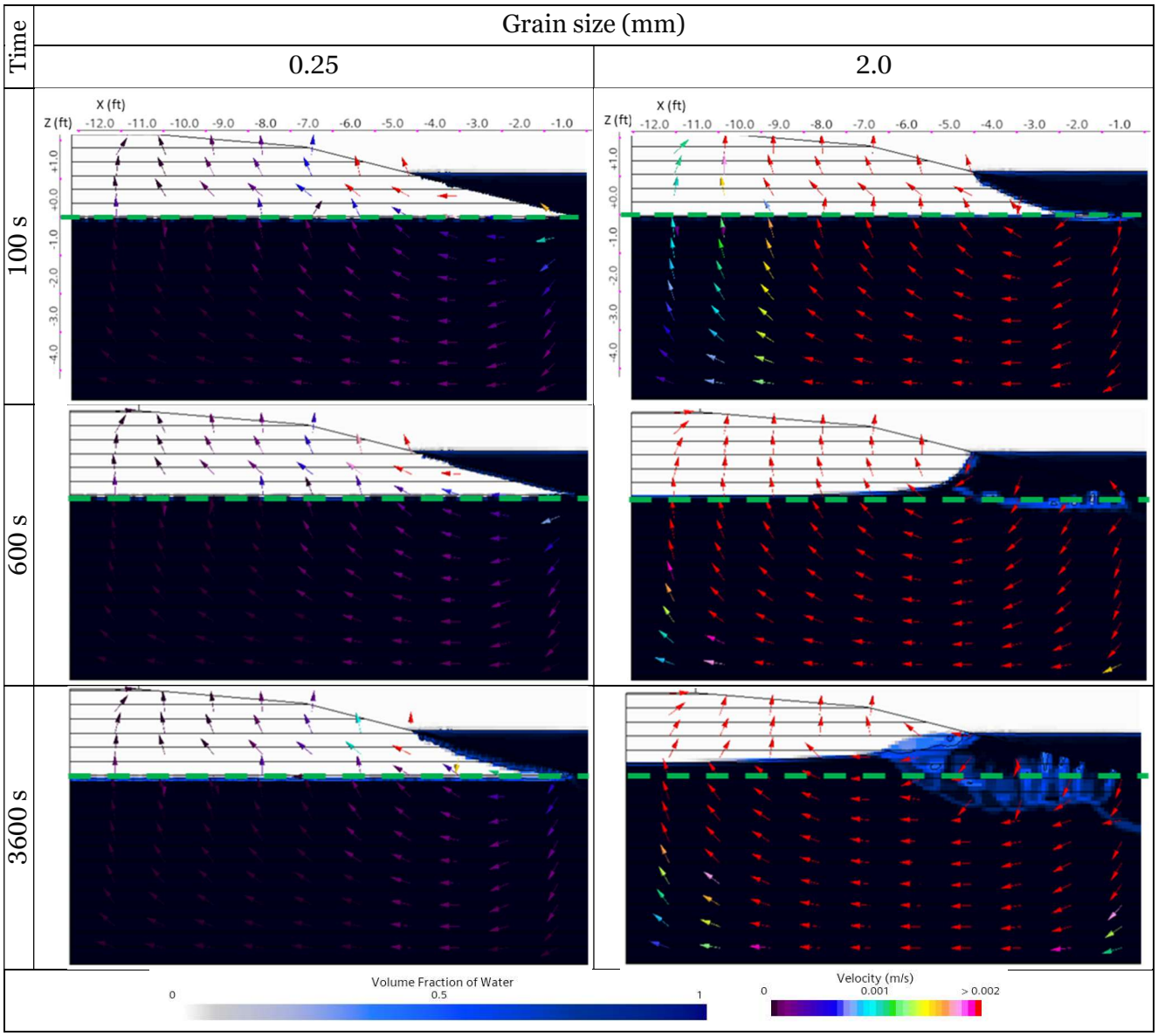



**Figure 4-14 Saturation at various times in a case with water table at the ditch bottom, soil porosity 5%, and grain size 0.25 mm and 2 mm.**

The analysis of results shows that the larger grains allow for a faster infiltration into the soil. At 95% compaction and 0.25-mm-size grains, the water table does not increase. For the case with 2-mm-size grains, water almost reaches the subbase within an hour of simulated time. Figure 4-14 shows the progress of infiltration within an hour of simulated time for both grain sizes. Within

this time, the infiltration does not reach the subbase. Figure 4-15 shows the saturation after 10 hours of simulated time for the model with 2-mm-size grains when the infiltrating water has already reached the bottom of the subbase. When porosity is 40%, the ground water reaches the subbase within approximately 1 hour of simulated time for the smaller sand grains as shown in Figure 4-16. With the underground water table occurring close to the surface, in the worst-case scenario the soil is fully saturated up to the water surface level in the ditch. Above the water table, the water content in the soil is non-zero over a distance due to the capillary rise, as discussed in Section 3.2.2, which suggests that a positive freeboard should be included in the design and its magnitude depends on the type of soil.

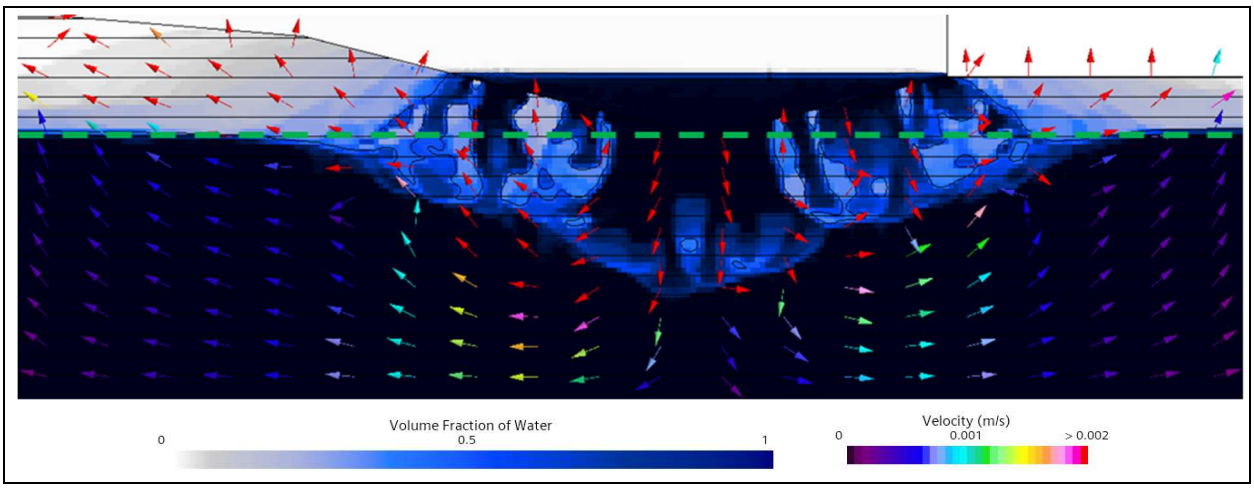



**Figure 4-15 Saturation at 10 hours of simulated time in the case with water table at the ditch bottom, soil porosity 5%, and grain size 2 mm.**

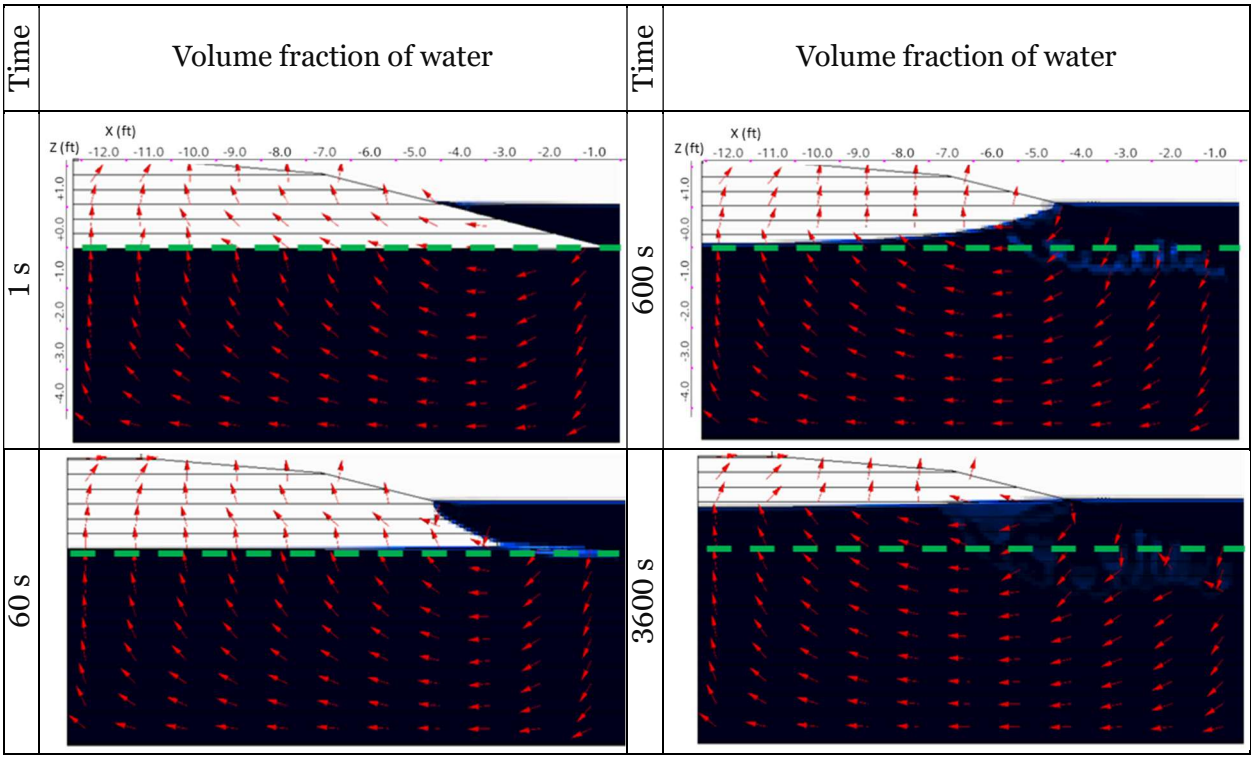



**Figure 4-16 Saturation at various times in a case with water table at the ditch bottom, soil porosity 40%, and grain size 0.25 mm.**

## 4.6 Comparison of CFD and VS2D Results

An evaluation of the CFD results was performed by comparison with the VS2D code for a set of conditions. Figure 4-17 presents the infiltration extent for grain size 1mm and porosity 5% at 1 hr of simulated time. The shape of the waterfront as well as its horizontal and vertical extent are very close in the two solutions; for example, the horizontal extent measured from the centerline of the ditch is ~2.2 m (7.2 ft) for CFD, and ~2.3 m (7.5 ft) for VS2D code.

Figure 4-18 shows infiltration extent after 1 hr for soil with grain size 0.1 mm, porosity 5% and Figure 4-19 for soil with grain size 2 mm and porosity 20%. In the first case, the results are very comparable; both models estimate an almost negligible infiltration within the tested time. In the second case, the water infiltrates soil further away from the ditch in the horizontal direction in the VS2D model than in the CFD model. Nevertheless, the result is similar close to the subbase.

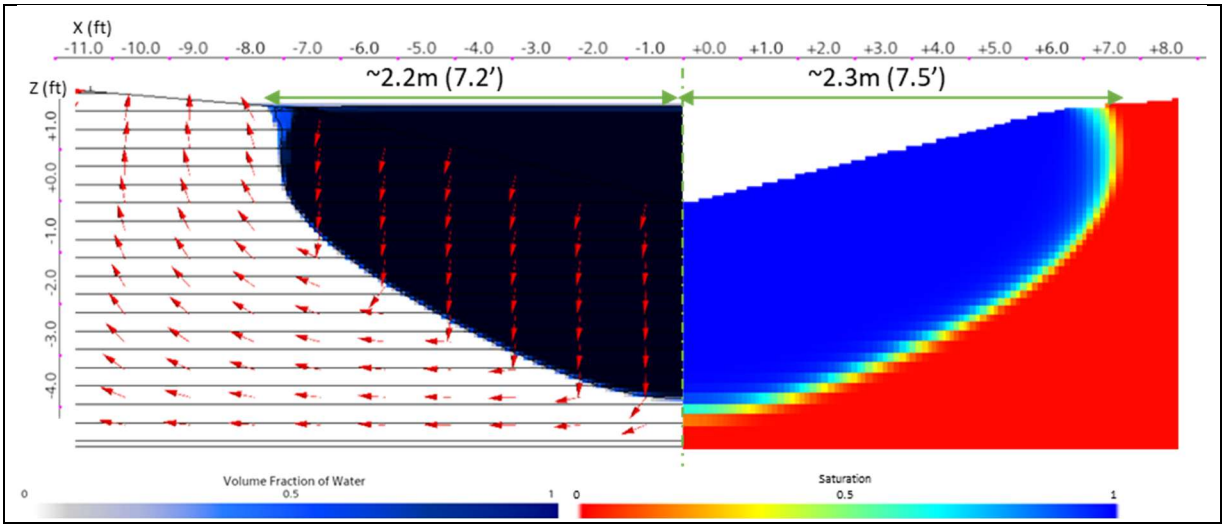



**Figure 4-17 Comparison of results from CFD and VS2D at 1hr of simulated time. Grain size 1 mm, soil porosity 5%. Note: the color bars differ between the software; blue color means full saturation in both codes; VS2D plot covers only the soil, and CFD covers both soil and the volume above it.**

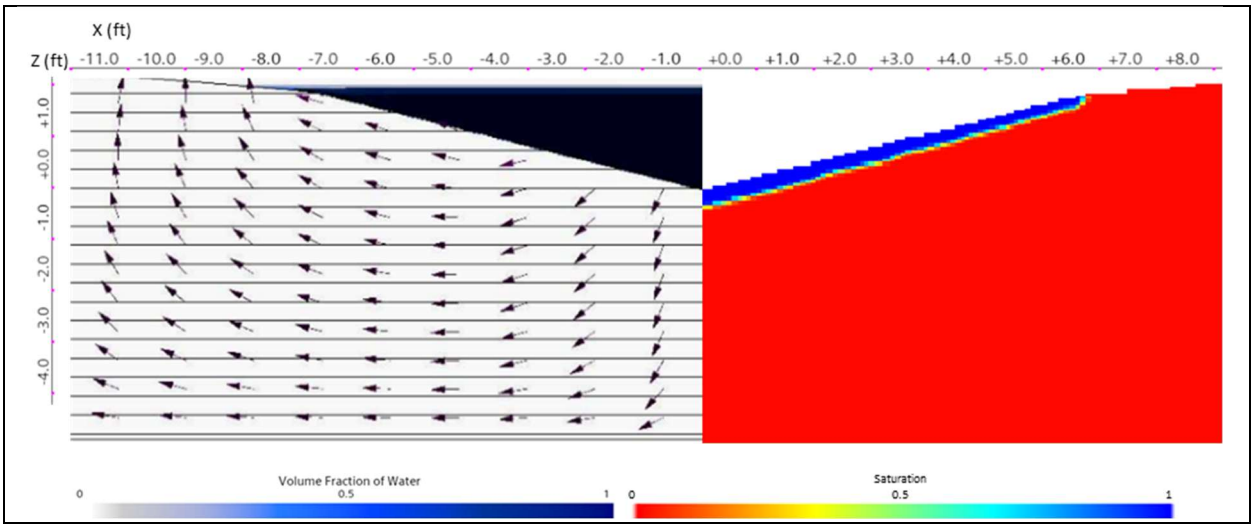



**Figure 4-18 Comparison of results from CFD vs. VS2D at 1hr of simulated time. Grain size is 0.1 mm, porosity 5%.**

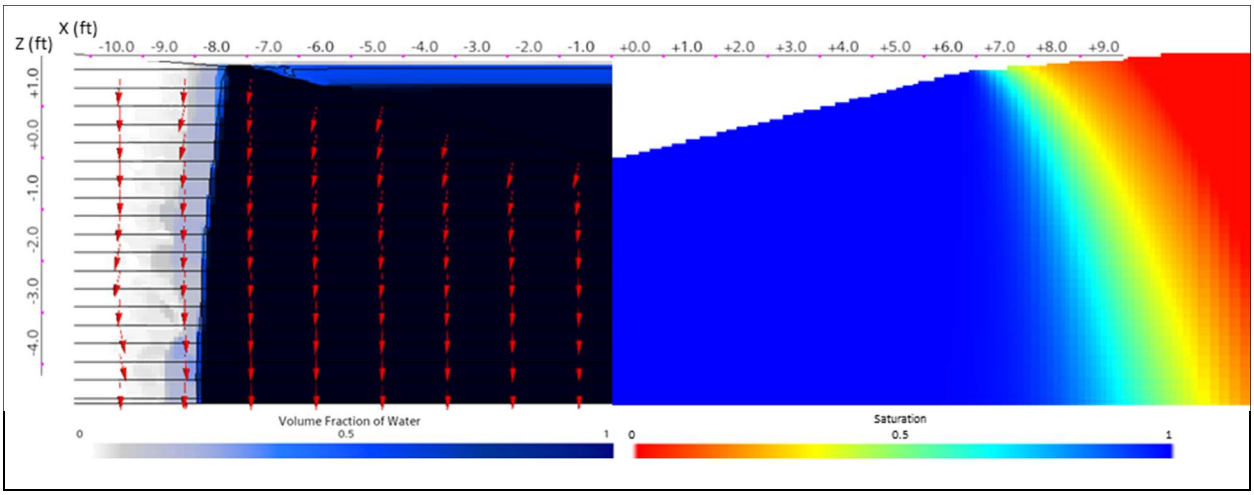



**Figure 4-19 Comparison of results from CFD vs. VS2D at 1hr of simulated time. Grain size is 2 mm, porosity 20%.**

The models built in VS2D software run much faster than those developed in the 3D CFD code. For this reason, the simulated time was extended in a few scenarios up to 24 hours. Figure 4-20 shows the infiltration progress at 1 hr and 24 hr of simulated time obtained from the VS2D software. At 24 hr, the maximum full saturation extent is 3.5 m (11.5 ft) at the bottom of the model. Water does not reach the subbase within this time. If the grain size is 0.01 mm at porosity 5%, even after 24 hr the infiltration is negligible as shown in Figure 4-21.

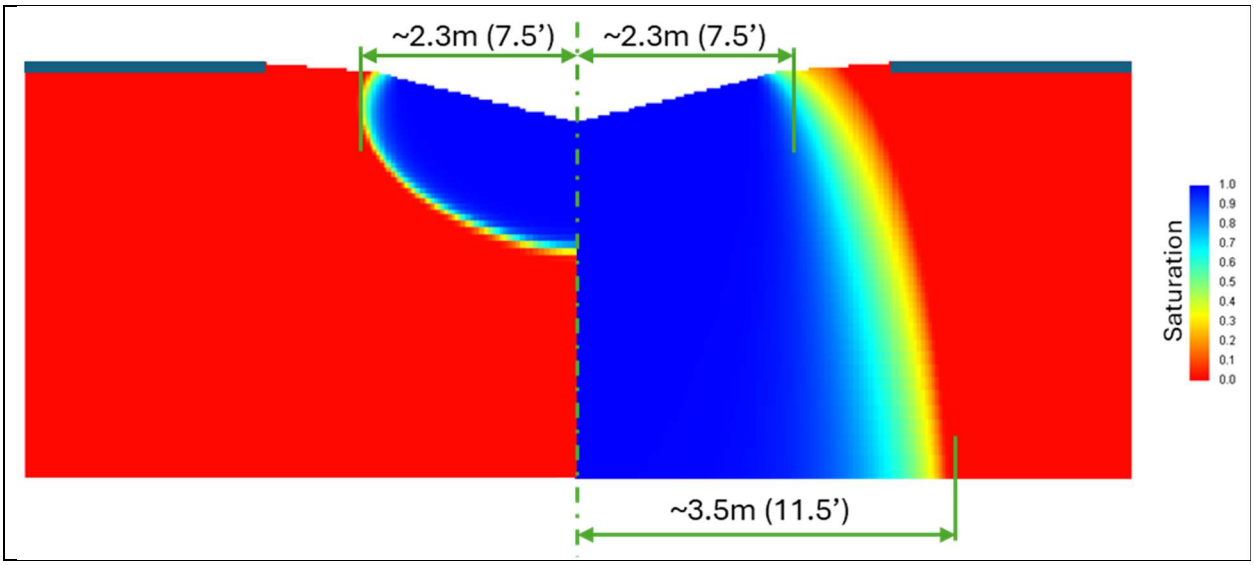



**Figure 4-20 Comparison of the infiltration at 1 hr (left) and 24 hr (right) of the simulation in VS2D. Grain size is 1 mm, soil porosity 5%.**

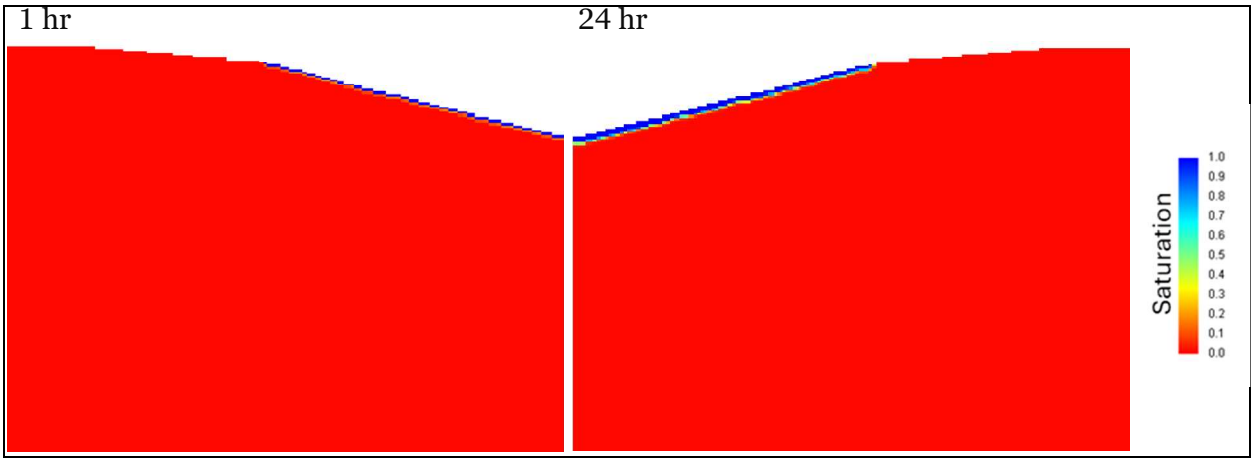



**Figure 4-21 Comparison of the infiltration at 1 hr (left) and 24 hr (right) of the simulation in VS2D. Grain size is 0.01 mm, porosity 5%.**

# 5 Conclusions

The CFD model used in this study represents a thin slice through the roadway, ditch, and the space above and below them. The geometry of the model assumes axial uniformity of the roadway and its surroundings. The water level in the ditch is kept constant throughout the simulation.

The soil volume is represented with a porous media model with resistance calculated as for a volume filled with spherical particles with size varied from 0.001 mm to 2 mm. It has non-zero porosity, and viscous and inertial resistance. In turn, the volume above the soil has a unit porosity and zero resistance to the flow. Both volumes may contain water and air defined with the phase volume fraction. This approach allows for representing unsaturated and saturated soils in the same model. Validity of using the porous media model for engineering CFD analysis was established by comparison with a physical test performed by Watson [22].

The model is not free of limitations, such as the assumption that the soil is made of spherical particles with a constant diameter. In reality, the shape of soil particles varies, which may impact the extent of the infiltration. Soils properties may vary with a gradation of the grain size and some of their characteristics depend on it. For example, hydraulic conductivity depends on the size of the smallest grains, and this property is commonly defined as a function of $d_{10}$. Also, the impact of vegetation was not included in the model.

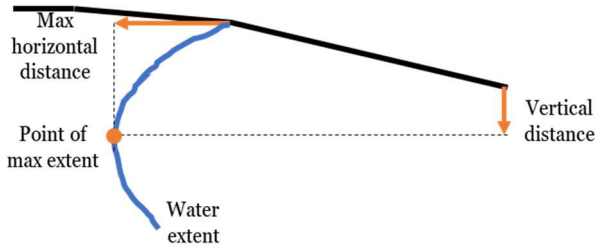
Nevertheless, the simulations performed during this study exhibit well-known characteristics of soil hydraulics: the compaction of the soil (decrease in porosity) decreases the infiltration speed and its horizontal extent. Also, soils made of finer particles infiltrate slower than when they consist of larger diameter grains.

No model for capillary rise in porous media is included in the used CFD software. However, an approach was implemented in which negative pressure is applied to the top surface of the soil volume. This soil boundary condition provides an equivalent of the capillary pressure and does produce some capillary rise. The results show that this modification slightly increases the infiltration extent but not enough to cause the moisture to reach the subbase. This means that it does not change the findings obtained from models without capillary pressure.

The CFD with porous media model results were compared with results from VS2D, a 2D code based on Richards' equations. The comparison shows that CFD and the VS2D codes give similar results in the scenarios considered. VS2D gives slightly bigger horizontal extent of the infiltration which results in a more conservative result. Also, the VS2D code gives results much faster than CFD and can be used on a personal computer. Unfortunately, it is not currently supported, and the latest version was released in 2012.

Table 5-1 summarizes the main findings of the study, namely the increase in the horizontal distance from the front slope and the corresponding vertical distance from the ditch bottom (positive values mean that the location is above the ditch bottom, and negative values mean that it is below).

**Table 5-1 Summary of results**

|  | Max increase in the horizontal extent from the front slope (ft) | Corresponding vertical distance from the ditch bottom (ft); above (+), below (-) |
|---|---|---|
| Grain size d=0.2 mm, porosity 40%, no initial moisture (base case) | +3/4 | +1/3 |
| Base case with added capillary pressure | +1.0 | +2/3 |
| Grain size 0.01 mm, porosity 0.05÷0.4, no initial moisture | negligible | n.a. |
| Grain size 2 mm, porosity 0.05÷0.4, no initial moisture | +5/4 | -4.0 |
| Grain size d<=0.1mm, porosity 5%, no initial moisture | negligible | n.a. |
| Grain size d=1mm, porosity 5%, no initial moisture | +3/4 | z>0 |
| Initial moisture 0÷0.3 | negligible | n.a. |
| Groundwater at ditch bottom, grain d=2mm, porosity 5% | groundwater level may increase to the water level in the ditch within a few hours | |
| Groundwater at ditch bottom, grain d=0.25mm, porosity 40% | groundwater level may increase to the water level in the ditch within less than 1 hr | |

The current South Carolina DOT design criteria require that the road subgrades be 1.0 foot above the design event water surface elevation in the ditch in order to lower the risk of pavement damage by moving the flow away from the pavement, containing the captured flow, and conveying flow received from adjacent properties to outfalls. It was found in the study that this guideline is reasonable within the scope of the study. The analyzed cross-section of the roadway and its vicinity leads to a conclusion that if a groundwater table at or close to the ditch bottom occurs, the vertical distance between the design water surface elevation in a ditch and the bottom of the road subbase should be greater than zero (positive freeboard). If the groundwater is not present or the table is lower than the ditch bottom, the limiting factor is the horizontal distance between the road and the ditch. Within the range of soil properties, geometries, and hydraulic boundary conditions considered in this study, a 10-ft horizontal separation from the ditch front slope to the pavement structure appeared sufficient to prevent infiltrating water from reaching the subbase during the simulated events, provided that a shallow groundwater table was not present.

Repeated saturation events may affect slope performance in ways not captured by the present hydraulic analysis. In addition to increasing moisture content, repeated wetting can reduce matric

suction, soften near-surface soils, and potentially contribute to seepage- or toe-related instability where slopes extend toward drainage ditches. These mechanisms were not explicitly evaluated in this study and should therefore be considered in site-specific geotechnical assessments. Interpretation of the results would also benefit from input from a geotechnical engineer familiar with local soil conditions, who can assess how closely the soils examined here represent field soils and which findings are most applicable in practice.

Based on the simulations conducted in this study, the following engineering implications are suggested:

1. Maintain current SCDOT design criteria for a positive freeboard where shallow (within 1 ft of the ditch) groundwater may be present. The groundwater cases indicate that when the mean groundwater table is near the ditch bottom, the risk increases that moisture or saturation will approach the roadway subbase. Where groundwater is expected near the ditch bottom, maintaining positive freeboard remains prudent.

2. Where groundwater is absent and lateral offset is sufficient, reduced freeboard may be acceptable within the tested conditions. For the roadway geometry and soil conditions examined, infiltration from the ditch tended to migrate mainly downward and did not reach the subbase when the lateral separation was at least about 10 ft which is consistent with current SCDOT design criteria for lateral offset/freeboard. This finding should be interpreted only within the range of conditions examined in this study.

3. Fine-grained and/or highly compacted soils showed limited infiltration during the simulated event durations. These soils generally produced smaller wetting-front extents and slower moisture migration than coarser, more permeable materials.

4. Additional geotechnical review is suggested where site conditions may increase risk, including:

    - coarse granular embankment soils,
    - long-duration ponding or sustained ditch flow,
    - repeated wetting events that may affect embankment or pavement performance.

5. Site screening for shallow groundwater should be considered if reduced freeboard is contemplated. Because groundwater conditions appear to be a controlling factor, any relaxation of current criteria would be better supported where shallow groundwater has been ruled out or shown to remain below critical elevations.

# 6 Acknowledgements

The funding for this project came from South Carolina DOT via Transportation Pooled Fund Program TPF-5(552), managed by the Turner-Fairbank Highway Research Center through the Interagency Agreement Number DTFH61-14-X-300002 between DOT and DOE, and the work was performed under DOE's contract with UChicago Argonne, LLC, contract no. DE-AC02-06-CH11357.

The authors gratefully acknowledge Mr. Tom Knight of the South Carolina Department of Transportation (SCDOT) for his continued support and engagement throughout this project. His extensive review of the report and numerous constructive comments contributed substantially to the improvement of both its technical content and clarity. The authors also wish to thank Mr. James Pagenkopf of the Turner-Fairbank Highway Research Center (TFHRC) for his helpful comments and input during the course of this work.

# 7 References


[1] SCDOT, Requirements for Hydraulic Design Studies, 2009
[2] USDA, Agriculture Handbook No. 18, the Soil Survey Manual, 2017
[3] Kellogg Soil Survey Laboratory Methods Manual, Soil Survey Investigations Report No. 42, Version 6.0 Part 1: Current Methods, 2022
[4] Brady, Nyle C, and Ray R Weil. *Elements of the Nature and Properties of Soils*. Upper Saddle River, N.J: Prentice Hall, 2004
[5] Revil A., Grauls D, Brevart O., Mechanical compaction of sand/clay mixtures, Journal of Geophysical Research, vol. 107, no. B11, 2293, 2002
[6] https://www.scdot.org/business/scdot-construction-manual.html
[7] https://www.scdot.org/business/pdf/materials-research/testProcedure/soils/SCT29.pdf
[8] https://www.scdot.org/business/pdf/materials-research/testProcedure/soils/SCT25.pdf
[9] https://webbook.nist.gov/chemistry/fluid/
[10] https://www.nrcs.usda.gov/Internet/FSE_DOCUMENTS/nrcs142p2_052523.pdf
[11] Hazen A. Discussion: dams on sand foundations. Trans Am Soc Civ Eng. 1911;73:199–203.
[12] J. Kozeny, Uber kapillare Leitung des Wassers im Boden Sitzungsber. Akad. Wiss. Wien, 136 (1927), pp. 271-306
[13] P.C. Carman, Fluid flow through a granular bed Trans. Inst. Chem. Eng., 15 (1937), pp. 150-156
[14] https://www.fao.org/4/r4082e/r4082e03.htm
[15] Hillel, D. (1998). Environmental Soil Physics. Academic Press.
[16] Kang, S.H., 2017. Development of mobilization criterion for debris flow and applicability assessment at a regional scale. Doctoral Thesis.
[17] R. W. Healy, H. I. Essaid : VS2DI: Model Use, Calibration, and Validation, Transactions of the ASABE (American Society of Agricultural and Biological Engineers), July 2012
[18] Nield, D. A., & Bejan, A. (2017). Convection in Porous Media (5th ed.). Springer.
[19] Ergun, Sabri. "Fluid flow through packed columns." Chem. Eng. Prog. 48 (1952).
[20] M. Th. Van Genuchten, A closed form equation for predicting the hydraulic conductivity of unsaturated soils, Soil Science Society of America Journal. Vol. 44, no.5, 1980
[21] SIEMENS, “Simcenter STAR-CCM+ Documentation Version 17.06.”, 2020
[22] K.K. Watson, An Instantaneous Profile Method for Determining the Hydraulic Conductivity of Unsaturated Porous Materials, Water Resources Research, vol.2, no.4, 1966
[23] James Jurin, An account of some experiments shown before the Royal Society; with an enquiry into the cause of some of the ascent and suspension of water in capillary tubes, *Philosophical Transactions of the Royal Society of London*, 30 , 1718
[24] White, L.R., Capillary rise in powders, Journal of Colloid and Interface Science, vol 90, no 2, 1982
[25] Hird R., Bolton M.D., Clarification of capillary rise in dry sand, Engineering Geology 230, 2017

www.anl.gov

## ARGONNE NATIONAL LABORATORY

- U.S. Department of Energy research facility
- Operated by the UChicago Argonne, LLC
- Midwest's largest federally funded R&D facility
- Located in Lemont, IL, about 25 miles (40 km) southwest of Chicago, IL (USA)
- Conducts basic and applied research in dozens of fields
- Unique suite of leading-edge and rare scientific user facilities

**CONTACT**
**Argonne National Laboratory**
9700 South Cass Avenue
Lemont, IL 60439
630-252-2000

U.S. DEPARTMENT of ENERGY

Argonne National Laboratory is a U.S. Department of Energy laboratory managed by UChicago Argonne, LLC.